

# Studies of novel phases and states produced by means of high pressure

Polymer and polymer based carbon nanocomposites

**Junchun Yu**

**喻俊淳**



Doctoral Thesis  
Department of Physics  
Umeå University, Sweden  
Umeå 2011

ISBN: 978-91-7459-315-0

Cover: Microstructures of carbon nanotube-polymer systems

Back: The partly reversible microstructure of a C<sub>60</sub>-polyisoprene composite

Electronic version available at: <http://umu.diva-portal.org/>

Printed by: Print&Media

Umeå, Sweden 2011

To Yuna 滢娜



## Abstract

This thesis concerns the thermal and mechanical properties of polymer and polymer based carbon nanocomposite materials, and the effect of treatments at high-pressure high-temperature (HP&HT) conditions. The study includes the nanofillers: single-wall carbon nanotube, SWCNT, multi-wall carbon nanotube, MWCNT and buckminsterfullerene,  $C_{60}$ . HP&HT treatments were used to significantly change crystallinity or cross-link density of the technologically important polymers: nylon-6, polyisoprene and polybutadiene, and study the effects on the polymer and polymer nanocomposite properties.

An *in-situ* transient hot-wire method was applied to measure simultaneously the thermal conductivity  $\kappa$  and heat capacity per unit volume, and to determine glass and phase transitions. Microscopic techniques, vibrational spectroscopy, thermal analysis, nuclear magnetic resonance and wide angle X-ray diffraction were applied to characterize the microstructural changes of samples caused by HP&HT treatments.

HP&HT treatment of the semicrystalline polymer nylon-6, increased the crystallinity from ca. 30% to as much as 60% for both nylon-6 and nylon-6 nanocomposites. Concurrently,  $\kappa$  increased ca. 40% because of increased crystallinity. Presence of MWCNTs produced a state with improved thermal stability and ~13% higher  $\kappa$  per weight percent carbon nanotube, CNT.

In a direct comparison, SWCNT fillers increased  $\kappa$  of amorphous polyisoprene slightly more than MWCNT fillers. This could be accounted for by the higher aspect ratio (length/diameter) of SWCNTs, whereas the two times higher  $\kappa$  of SWCNTs affected the composite's  $\kappa$  to a much lesser extent.

HP&HT treatment of polyisoprene and polybutadiene, and their nanocomposites caused cross-linking of the polymer chains, but no evidence suggested that CNTs were covalently bonded to the polymer. The cross-links increased  $\kappa$  of the recovered states by up to 50% at ambient conditions, and improved the thermal and mechanical stability of the polymers and their nanocomposites.

Addition of CNTs or  $C_{60}$  in polyisoprene significantly improved the tensile strength by 38% and 49%, respectively, per weight percent filler after cross-linking at HP&HT conditions. The CNT/polyisoprene composite appears to be reinforced via an efficient load transfer supplied by strongly bonded polymer chains wrapped/coated on the CNTs, whereas the  $C_{60}$ /polyisoprene composite was reinforced via covalent bonding between  $C_{60}$ -polyisoprene and  $C_{60}$ - $C_{60}$ . Interestingly, the  $C_{60}$ - $C_{60}$  bonds can be broken by heating at ambient pressure, which facilitates recycling.



## Sammanfattning

Denna avhandling berör termiska och mekaniska egenskaper hos polymerer och polymerbaserade kolnanokompositer, och effekten av behandling vid höga tryck och höga temperaturer (HP&HT). I studien ingår nanofillerna: enkelväggiga kolnanorör, SWCNT, flerväggiga kolnanorör, MWCNT och buckminsterfulleren, C<sub>60</sub>. HP&HT behandling användes för att väsentligt ändra kristalliniteten eller tvärbindingstätheten för de teknologiskt viktiga polymererna: nylon-6, polyisopren och polybutadien, och studera effekterna på polymerernas och polymera nanokompositernas egenskaper.

En *in-situ* varmtrådsmetod användes för att simultant mäta både värmeledningsförmågan  $\kappa$  och värmekapaciteten per volymenhet, samt för att bestämma glas och fasövergångar. Mikroskopiska tekniker, vibrationsspektroskopi, termisk analys, kärnmagnetisk resonans och röntgendiffraktion tillämpades för att karaktärisera provens mikrostruktur före och efter HP&HT behandlingar.

Vid HP&HT behandling av den semikristallina polymeren nylon-6 ökade kristalliniteten från ca. 30% till så mycket som 60% för både nylon-6 och nylon-6 nanokompositer. Samtidigt ökade  $\kappa$  ca. 40% tack vare den ökade kristalliniteten. Inblandning av MWCNTs producerade ett tillstånd med större termisk stabilitet och ca. 13% högre  $\kappa$  per viktprocent kolnanorör. Vid en direkt jämförelse ökade  $\kappa$  mer vid inblandning av SWCNTs i amorf polyisopren än vid inblandning av MWCNTs. Detta kan förklaras av högre aspect ratio (längd/diameter) för SWCNTs medan deras två gånger högre  $\kappa$  påverkar i betydligt mindre utsträckning.

I polyisopren och polybutadien och deras nanokompositer orsakade HP&HT behandling tvärbindingar mellan polymerkedjorna, men inga resultat indikerade kovalenta bindningar mellan kolnanorören och kedjorna. Tvärbindingarna ökade  $\kappa$  med upp till 50% vid normala förhållanden och förbättrade termiska och mekaniska stabiliteten för polymererna och deras nanokompositer.

Inblandning av kolnanorör eller C<sub>60</sub> i polyisopren gav signifikant förbättrad draghållfasthet på, respektive, 38% och 49% per viktprocent filler efter tvärbinding genom HP&HT behandling. Resultat tyder på att kolnanorörskompositen förstärks genom en effektiv lastöverföring när polymerkedjorna binds starkt på ytan av kolnanorören genom beläggning, medan C<sub>60</sub> kompositen förstärktes genom kovalenta bindningar mellan C<sub>60</sub>-polyisopren och C<sub>60</sub>-C<sub>60</sub>. En intressant effekt är att C<sub>60</sub>-C<sub>60</sub> bindningarna kan brytas upp genom uppvärmning vid normalt tryck, vilket underlättar återvinning av kompositen.



## Included papers

This dissertation is based on the following publications, which are categorized according to topic and attached at the end of this thesis:

### **I. “High-Pressure-Induced Microstructural Evolution and Enhancement of Thermal Properties of Nylon-6”**

**Junchun Yu**, Bounphanh Tonpheng and Ove Andersson

*Macromolecules* **2010**, 43, 10512-10520.

DOI: 10.1021/ma102273b

### **II. “Thermal Properties and Transition Studies of Multi-Wall Carbon Nanotube/Nylon-6 Composites”**

**Junchun Yu**, Bounphanh Tonpheng, Gerhard Gröbner and Ove Andersson

*Carbon* **2011**, 49, 4858-4866.

DOI: 10.1016/j.carbon.2011.07.006

### **III. “Microstructure, Nucleation and Thermal Properties of High-Pressure Crystallized MWCNT/Nylon-6 Composites”**

**Junchun Yu**, Gerhard Gröbner, Bounphanh Tonpheng, and Ove Andersson

*Polymer* **2011**, 52, 5521-5527

DOI:10.1016/j.polymer.2011.09.036

### **IV. “Thermal Conductivity, Heat Capacity, and Cross-Linking of Polyisoprene/Single-Wall Carbon Nanotube Composites under High Pressure”**

Bounphanh Tonpheng, **Junchun Yu** and Ove Andersson

*Macromolecules* **2009**, 42, 9295-9301.

DOI: 10.1021/ma902122u

### **V. “Tensile Strength and Young's Modulus of Polyisoprene/Single-Wall Carbon Nanotube Composites Increased by High Pressure Cross-linking”**

Bounphanh Tonpheng, **Junchun Yu**, Britt M. Andersson and Ove Andersson

*Macromolecules* **2010**, 43, 7680-7688.

DOI: 10.1021/ma101484e

**VI. “A MWCNT/Polyisoprene Composite Reinforced by an Effective Load Transfer Reflected in the Extent of Polymer Coating”**

**Junchun Yu**, Bounphanh Tonpheng, Gerhard Gröbner and Ove Andersson  
Submitted

**VII. “Effects of Cross-Links, Pressure and Temperature on the Thermal Properties and Glass Transition Behaviour of Polybutadiene”**

Bounphanh Tonpheng, **Junchun Yu** and Ove Andersson  
*Physical Chemistry Chemical Physics* **2011**, 13, 15047-15054.  
DOI: 10.1039/C1CP20785G

**VIII. “Microstructural and Property Changes in High Pressure Treated Carbon Nanotube/Polybutadiene Composites”**

**Junchun Yu**, Bounphanh Tonpheng, Gerhard Gröbner and Ove Andersson  
*Journal of Materials Chemistry* **2011**, 49, 13672-13682.  
DOI: 10.1039/C1JM12187A

**IX. “Buckminsterfullerene: a Strong, Covalently Bonded, Reinforcing Filler and Reversible Cross-Linker in the Form of Clusters in a Polymer”**

**Junchun Yu**, Gerhard Gröbner, Bounphanh Tonpheng, and Ove Andersson  
In manuscript

Conference Proceedings, which are **not** included in this thesis:

**1. “Polyisoprene Single-Wall Carbon Nanotube Composites Synthesized under High Pressure”**

Bounphanh Tonpheng, **Junchun Yu** and Ove Andersson  
*High Pressure Research*, Volume 28, Issue 4, 2008, pp. 587-590  
Proceedings of the 46th European high pressure research group (EHPRG 46)  
meeting, 7–12 September 2008, Valencia, Spain

**2. “Thermal Conductivity and Heat Capacity of a Nylon-6/Multi-Wall Carbon Nanotube Composite under Pressure”**

**Junchun Yu**, Bounphanh Tonpheng and Ove Andersson  
*AIP Conference Proceedings*, Volume 1255, June 2, 2010, pp. 145-147  
5th international conference on times of polymers (TOP) and composites,  
20-23 June 2010, Ischia, Italy

# Table of Contents

<b>Abbreviations</b>	<b>xiii</b>
<b>I. Introduction and motivation</b>	<b>1</b>
<b>1. Introduction</b>	<b>1</b>
1.1 Motivation of this thesis work	3
<b>II. Experiment techniques and materials</b>	<b>4</b>
<b>2. Carbon nanotube</b>	<b>4</b>
2.1 A brief introduction	4
2.2 SWCNTs and MWCNTs used in this thesis	6
2.3 Purification of MWCNTs	7
<b>3. Buckminsterfullerene</b>	<b>8</b>
3.1 A short history	8
3.2 Specification of C <sub>60</sub> in this research	9
<b>4. The polymers and composite material</b>	<b>10</b>
4.1 Nylon-6	10
4.2 Polyisoprene (PI) and Polybutadiene (PB)	11
4.3 The CNT based composite material: achievement and challenge	12
4.4 Covalently bonded C <sub>60</sub> -PI composites	14
<b>5. Sample synthesis and preparation</b>	<b>15</b>
5.1 <i>In-situ</i> polymerization	15
5.2 Solvent mixing	15
5.3 Sample preparation	16
5.3.1 <i>Hot press</i>	16
5.3.2 <i>Spin coating</i>	17
<b>6. <i>In-situ</i> sample characterization</b>	<b>18</b>
6.1 High pressure equipments and their functions	18
6.1.1 <i>Press family</i>	18
6.1.2 <i>Piston-cylinder apparatus and Teflon<sup>®</sup> cells</i>	18
6.1.3 <i>Support electronics and program</i>	20
6.2 <i>In-situ</i> transient hot-wire measurement	20
6.2.1 <i>A brief introduction to thermal conductivity <math>\kappa</math></i>	21
6.2.2 <i>Transient hot-wire method: the theory</i>	22
6.2.3 <i>Experimental setup of hot-wire measurement</i>	23
6.2.4 <i>The details of calculation of <math>\kappa</math> and <math>\rho C_p</math></i>	25
6.3 <i>In-situ</i> differential thermal analysis	26
6.4 High-pressure high-temperature treatment	26
<b>7. Tensile measurement</b>	<b>27</b>
7.1 Tensile properties of polymer based composite material	27
7.2 Experimental setup	28
7.3 Repeatability and calibration of tensile tester	29
<b>8. Sample characterization</b>	<b>30</b>

8.1 Atomic force microscope	30
8.1.1 <i>Contact mode AFM</i>	31
8.1.2 <i>Tapping mode AFM</i>	32
* <i>Phase image</i>	32
8.1.3 <i>Sample preparation</i>	33
8.1.4 <i>The probes and images</i>	34
* <i>LTESP</i>	34
* <i>RTESP</i>	34
* <i>MSNL</i>	34
* <i>OSCM</i>	35
* <i>Image artifacts</i>	35
8.2 Transmission electron microscope	35
8.2.1 <i>TEM sample preparation: ultramicrotome sectioning</i>	36
8.3 Scanning electron microscope	38
8.3.1 <i>Sample preparation: coating with gold</i>	38
8.4 Optical microscope	38
8.5 Nuclear magnetic resonance	39
8.5.1 <i>Chemical shift</i>	40
8.5.2 <i>Magic angle spinning</i>	41
8.5.3 <i>Cross-polarization</i>	41
8.5.4 <i>Measurement of spin-spin relaxation time</i>	42
8.6 Wide angle X-ray diffraction	43
8.7 Vibrational spectroscopy	44
8.7.1 <i>Raman spectroscopy</i>	44
8.7.2 <i>Fourier transform infrared spectroscopy</i>	46
8.8 Differential scanning calorimetry	47
8.9 Cross-link density measurement	49
8.9.1 <i>Cross-link density via swelling</i>	49
8.9.2 <i>Cross-link density via Young's modulus</i>	50
8.9.3 <i>Cross-link density via NMR</i>	50
8.9.4 <i>Cross-link density via gel formation</i>	50
8.10 Viscosity measurement	50
8.11 Density measurement	52
<b>III. Summary of the included papers</b>	<b>53</b>
Paper I, II and III	53
Paper IV, V and VI	54
Paper VII and VIII	56
Paper IX	57
<b>IV. Conclusion and Perspective</b>	<b>58</b>
<b>Conclusion</b>	<b>58</b>
<b>Perspective</b>	<b>59</b>
<b>V. Supplementary material</b>	<b>60</b>
<b>9. Conferences, summer schools and other activities</b>	<b>60</b>

9.1 Conference	60
9.2 Summer school	60
9.3 Student networking activities	60
<b>Acknowledgements</b>	<b>61</b>
<b>References</b>	<b>63</b>



## Abbreviations

$\Delta H$	Melting (Total) enthalpy
$\varepsilon_B$	Tensile strain at break (elongation at break)
$\kappa$	Thermal conductivity
$\nu_E$	Cross-link density via Young's modulus $E$
$\nu_{\text{NMR}}$	Cross-link density via NMR
$\nu_{\text{swell}}$	Cross-link density via swelling
$\rho c_p$	Heat capacity per unit volume
$\sigma_{\text{UTS}}$	Ultimate tensile strength
AFM	Atomic force microscope
ATR	Attenuated total reflection
$B_0$	Permanent magnetic field
$C_{60}$	Buckminsterfullerene
CCD	Charge coupled device
CNT	Carbon nanotube
CP	Cross polarization
CSP	Crystallite size and perfection
CVD	Chemical vapor deposition
DSC	Differential scanning calorimetry
$E$	Young's modulus
EFM	Electrostatic force microscope
FID	Free induction decay
FTIR	Fourier transform infrared spectroscopy
HP&HT	High-pressure high-temperature
LPB	Polybutadiene with $M_r$ of 100 000
LPI	Polyisoprene with $M_w$ of 800 000
MAS	Magic angle spinning
$M_c$	Average molecular weight between cross-links
MD	Molecular dynamic
MFM	Magnetic force microscopy
$M_r$	Approximate relative molecular mass
$M_w$	Molecular weight
MWCNT	Multi-wall carbon nanotube
$M_{XY}$	Transverse magnetization
$M_Z$	Longitudinal (initial) magnetization
NMR	Nuclear magnetic resonance
OM	Optical microscope
PB	Polybutadiene
PE	Polyethylene

PI	Polyisoprene
PID	Proportional–integral–derivative
PP	Polypropylene
ppm	Parts per million
SDS	Sodium dodecyl sulfate
(HR-)SEM	(High-resolution) Scanning electron microscope
sPB	Polybutadiene with $M_r$ of 2600
sPI	Polyisoprene with $M_r$ of 38 000
SWCNT	Single-wall carbon nanotube
$T_1$	Spin-lattice relaxation time
$T_2$	Spin-spin relaxation time
$T_{\text{cry}}$	Recrystallization temperature
(HR-)TEM	(High-resolution) Transmission electron microscope
$T_g$	Glass transition temperature
$T_{\text{melt}}$	Melting temperature
TMS	Tetramethylsilane
$T_{\text{onset}}$	Melting onset temperature
WAXD	Wide angle X-ray diffraction

# I. Introduction and motivation

## 1. Introduction

Let us begin this thesis with element carbon (C), the 4<sup>th</sup> most abundant element in universe by mass, which is presented in various forms in nature, including both organic (oil, coal, etc.) and inorganic material (limestones, carbon dioxide, etc.). Carbon forms more compounds than any other element. It is presents in all known life forms, making it the chemical basis of all known life. [1] Besides forming various compounds, there are several types of allotropes of carbon, e.g. diamond, graphite, carbon black (amorphous carbon), carbon nanotube (CNT), [2] fullerenes, [3] and graphene [4] etc, with distinct differences in physical properties because of difference in carbon configuration. Among these materials, diamond and graphite are the best-known examples with widely different hardness, thermal conductivity and electrical conductivity due to different hybridization ( $sp^3$  or  $sp^2$  hybridized) of carbon. [2]

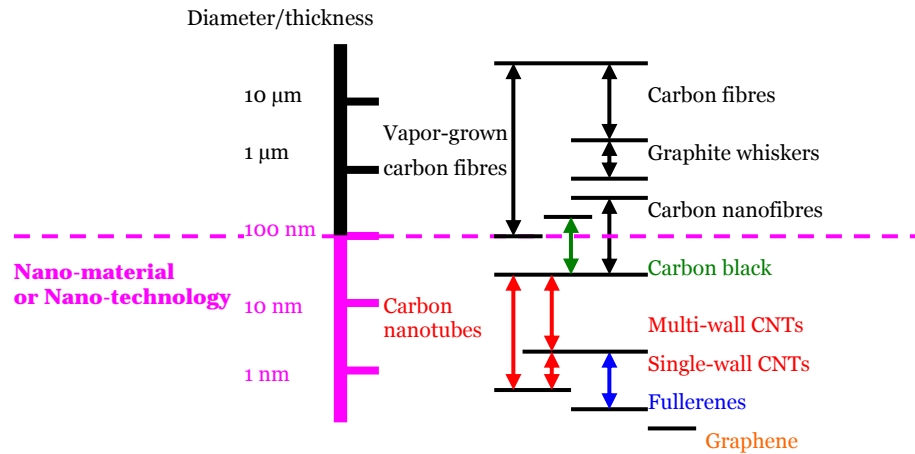


Figure 1.1: Size distribution of various allotropes of carbon: carbon fiber, carbon black, CNTs, fullerenes and graphene. [5]

Fullerenes and carbon nanotubes are interesting allotropes of carbon. [2] In 1980s, buckminsterfullerene (or  $C_{60}$ ), which is one member in the fullerene family, was first discovered by Smalley and his colleagues. [6] Later in the early 1990s, CNTs (including multi-wall carbon nanotube, MWCNT [7] and single-wall carbon nanotube, SWCNT [8]) were discovered and

acknowledged by the scientific community after the publications by Iijima. The extraordinary mechanical, thermal and electrical properties (see more details about the properties of CNTs and C<sub>60</sub> in Chapter. 2, 3) of CNTs provide many scientifically interesting and technologically useful possibilities, not only for the pure form [9-12] but also as an additive in composite systems, e.g. as a filler in polymer composites.

The use of fillers to change the properties of polymers has a long history and the method has been applied to enhance the performance of a matrix and to combine the useful properties of fillers and matrixes, especially when the filler is difficult to process or too expensive to use in the pure form. [13-15] As generally accepted by the science community, a particle having at least one dimension smaller than 100 nm is called a nanomaterial, and the science and technology of these materials are called nanoscience and nanotechnology (Figure 1.1). Consequently, C<sub>60</sub> which has a spherical shape with a diameter of less than 1 nm, and CNTs which have a tubular shape with a diameter of typically <10 nm are nano-sized fillers. Besides, a CNT has a typically large aspect ratio<sup>1</sup> (~10<sup>3</sup> for SWCNT), resulting in an extraordinarily large surface area (~1300 m<sup>2</sup> g<sup>-1</sup> for SWCNT).

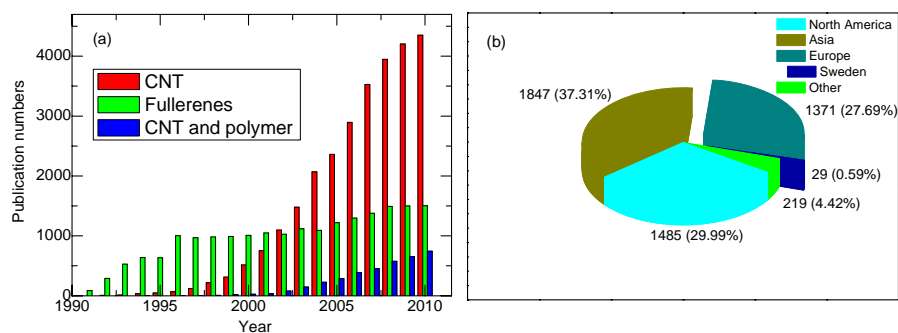


Figure 1.2: The numbers of publications of scientific papers sorted by (a) publication year or (b) territory. The data are returned from web of science® by searching using the keywords ‘CNT’, ‘fullerenes’ or ‘CNT and polymer’ in the topic line.

Results from a search in the Web of Science® database, using the keyword ‘CNT’, show that the number of studies of CNTs increases steadily after their discovery in 1990 (Figure 1.2a). The research on ‘CNT and polymer’ started in the middle of 1990’s, but did not boom until 2000’s after CNTs became available in larger quantities and the potential of using CNTs as additives in polymer composites was more widely known. The number of publications

<sup>1</sup> The ratio between length and diameter of CNT

was initially not very large but has increased rapidly during the last decade, from less than 100 in 2000 to more than 700 in 2010. The studies on fullerenes have a somewhat longer history. Since the discovery in 1980s, the publication number kept almost constant (ca. 1000 per year) with a slight increase after 2000. If one sorts the number of publications of 'CNT and polymer' by territory (Figure 1.2b), then Asia (37%), North America (30%) and Europe (28%) make up the three largest contributions. Surprisingly, Sweden has only contributed with 29 publications.

### **1.1 Motivation of this thesis work**

This thesis mainly concentrates on studies of the novel states of carbon nanotube (or C<sub>60</sub>)/polymer composites produced by/during high pressure high temperature (HP&HT) treatments and, in particular, the thermal conductivity and tensile properties of the composites.

The main objectives of this thesis work were as follows:

1. Introducing a unique technique -high-pressure high-temperature (HP&HT) studies (treatment)- to investigate the changes in CNT (or C<sub>60</sub>) filled polymer composite material.

2. Studying the dynamics and phase transition of various polymer and CNT filled polymer composites by *in-situ*  $\kappa$  and heat capacity per unit volume ( $\rho c_p$ ) measurements. The dynamics and phase transition include the glass transition behavior and its pressure-dependence, cold-crystallization and cross-linking processes of materials.

3. Characterizing the interaction between filler and polymer matrix before and after HP&HT treatment, and establishing whether or not the filler was covalently bonded to the polymer matrix after treatment. Besides, the structure-property relation, e.g. the HP&HT modified microstructure and corresponding tensile and thermal properties were investigated. In addition, the study includes the effect of filler on the thermal properties, e.g. melting temperature ( $T_{\text{melt}}$ ), recrystallization temperature ( $T_{\text{cry}}$ ) etc. and crystallization behavior of a semi-crystallized polymer matrix.

## II. Experiment techniques and materials

### 2. Carbon nanotube

#### 2.1 A brief introduction

CNT is a long-tubular shaped, cylindrical like structure consisting of pure carbon atoms, which also could be simply considered as a seamless roll-up of a graphene sheet. CNT could be naturally sub-divided to SWCNT (Figure 2.1, left) and MWCNT (Figure 2.1, right). SWCNT consists of only a layer of roll-up graphene sheet, whereas MWCNT may consist of more than 2 layers of these roll-up sheets arranged concentrically.

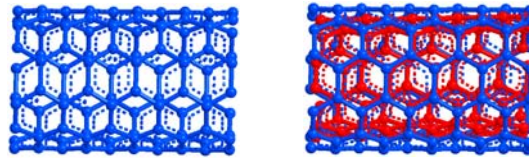


Figure 2.1: A schematic plot of a SWCNT (left) and a MWCNT (right).

CNTs are interesting because of their nano-sized diameter and micrometer length in combination with extraordinary thermal and mechanical properties, and high electrical conductivity, as shown in Table 2.1. This gives CNTs a great potential to be utilized in thermal management, high performance composites, electronic application etc. [13, 16-18]

Table 2.1: A summary of properties of SWCNT and MWCNT.

Properties	SWCNT		MWCNT	
	Theoretical	Experimental	Theoretical	Experimental
Thermal conductivity ( $W m^{-1} K^{-1}$ )	~7000 [19, 20]	>2000 [21]	---	>3000[22]
Tensile strength ( $\sigma_{UTS}$ , Pa)	~200 GPa [23, 24]	~350 GPa [25]	~200 GPa [24]	~28 GPa [26]
Young's modulus ( $E$ , Pa)	~1 TPa [24, 27, 28]	~7 GPa [25]	~1 TPa [24, 27]	~1 TPa [26, 29]
Specific surface area ( $m^2 g^{-1}$ )	1315 [30]	285 [31]	200 [30]	178 [32]
			(10 nm outer diameter)	
Electrical conductivity ( $S m^{-1}$ )		~1 [33]		~ $2 \times 10^3$ [34]
Diameter (nm)		Less than 2		From 10 to ca. 50
Density ( $g cm^{-3}$ )		1.3-1.5 [35]		1.8-2.0 [35]
Aspect ratio <sup>a</sup> (length/diameter)		~1000		~100
Price		Ca. €300 per gram (C purity >90% <sup>b</sup> )		Ca. €50 per gram (C purity >95% <sup>c</sup> )
Dispersibility		Difficult to disperse into single tube		Easy to disperse into single tube
Purities of material		Difficult to achieve high purity		Easy to achieve high purity

a. assuming a CNT length of 1  $\mu m$

b. information from Carbon Solution Inc, USA

c. information from Nanocyl, Belgium

In this thesis, I focus on the potential of CNTs to enhance the thermal, mechanical and electrical properties of a polymer matrix. Here I summarize briefly the reported experimental and simulated results for  $\kappa$ , tensile and electrical properties of CNTs.

Fujii et al. [21] measured  $\kappa$  of individual SWCNT and found  $\kappa > 2000 W m^{-1} K^{-1}$  for a CNT with a diameter of 9.8 nm. Kim et al. [22] found  $\kappa > 3000 W m^{-1} K^{-1}$  for individual MWCNT at room temperature while that of bundled CNTs has been reported as  $\sim 35 W m^{-1} K^{-1}$  for randomly orientated SWCNTs,  $\sim 200 W m^{-1} K^{-1}$  for aligned SWCNTs and  $\sim 20 W m^{-1} K^{-1}$  for randomly oriented MWCNTs. [36-39] Theoretically, it has been predicted that  $\kappa$  of a SWCNT can be as high as  $\sim 7000 W m^{-1} K^{-1}$  at room temperature. [19, 20] CNTs are the strongest and stiffest materials known so far. The SWCNT obtained a  $\sigma_{UTS}$  and  $E$  of  $\sim 7$  and  $\sim 350$  GPa respectively for a 19 nm bundle [25] where MWCNT had a  $\sigma_{UTS}$  of 28 GPa for a 13 nm MWCNT and  $E$  range from  $\sim 270$  to 950 GPa [26] or an average of 1.8 TPa reported by Treacy et al.

[29]. In general, theoretical calculations for SWCNTs and MWCNTs indicate even higher strength, and typically show  $\sigma_{UTS}$  and  $E$  values of order of  $\sim 1$  TPa. [27, 35] Moreover, the CNTs are good electrical conductors. Lee et al. [33] reported the electrical conductivity of  $\sim 1 \text{ S m}^{-1}$  for bundles of SWCNTs whereas Ebbesen et al. [34] reported the electrical conductivity of  $\sim 2 \times 10^3 \text{ S m}^{-1}$  for a MWCNT with diameter of  $\sim 20 \text{ nm}$ . In addition, the unique geometry of a CNT, i.e., high aspect ratio ( $\sim 10^3$ ) and low density ( $1 \sim 2 \text{ g cm}^{-3}$ ), makes it an ideal filler for fabricating lightweight composites with high strength and stiffness. [14, 40]

The major routes to synthesize CNTs include: arc discharge, laser ablation and chemical vapor deposition (CVD). [9, 41] In general, the fabrication processes involve transforming carbon-contained media, either in gas or solid state, into CNTs through a high-temperature, physical or chemical process with the help of catalysts. Briefly, arc discharge is a method where CNTs are produced in a carbon deposit on a negative (carbon) electrode after vaporization of carbon caused by high discharge temperatures. It is also the most widely used method since CNTs were initially discovered using this technique. [42] In the laser ablation process, a graphite target is vaporized by a pulsed laser in a high-temperature chamber containing an inert gas. The CNTs grow on cold surfaces of the reactor as the vaporized carbon condenses. In the CVD process, a metal catalyst coated substrate is heated to approximately  $700^\circ\text{C}$ . A process gas (ammonia, nitrogen or hydrogen) and a carbon-containing gas (acetylene, ethylene, ethanol or methane) are blended into the chamber to trigger the growth of CNTs at the sites of the metal catalyst. Recently, a high yield super-growth CVD process was developed by Hata et al. [43] In this process, highly dense, aligned CNT "forests", perpendicular to the substrate, were produced. The length of the forests can reach millimeter scale. Moreover, the growth efficiency is about 100 times higher than the laser ablation method.

## **2.2 SWCNTs and MWCNTs used in this thesis**

The SWCNTs with 4–7 wt % metal impurities and a carbonaceous purity of  $>90\%$  were produced by electric arc-discharge by Carbon Solution Inc, USA. The SWCNTs had a stated diameter of  $1.4 \text{ nm}$ . The average length was ca.  $1 \mu\text{m}$  in bundles of  $\sim 5 \text{ nm}$  in diameter, as observed in transmission electron microscopy (TEM) after high power sonication (VCX 130, 130W, 20 kHz, Sonics & Materials INC) in toluene for 30 minutes. The material was used without further purification.

MWCNTs produced by catalytic CVD were purchased from Nanocyl (3150, 3151 and 3154), Belgium. Nanocyl 3150 (non-MWCNT: non-functionalized

MWCNT), Nanocyl 3151 (MWCNT-COOH<sup>2</sup>: functionalized with less than 4% of -COOH) and Nanocyl 3154 (MWCNT-SH: functionalized with 0.5-1% -SH) have a stated diameter of 10 nm, carbon purity of >95% and a metal oxide content of <5%. TEM analyses showed that non-MWCNT and MWCNT-SH have a length of ca. 1  $\mu\text{m}$  and a diameter of ca. 10 nm in single tube form after high power sonication in toluene for 30 minutes whereas MWCNT-COOH have average lengths of  $\sim 0.5 \mu\text{m}$ . The MWCNT-COOH and MWCNT-SH were used without further treatment. In the studies of MWCNT/nylon-6 composites (Paper II, III), the non-MWCNT was purified (denoted as P-MWCNT<sup>3</sup>) before *in-situ* polymerization. But, as observed later in TEM, the non-MWCNT has fairly good purity, therefore the non-MWCNT was used as purchased in MWCNT/PI (Paper VI) studies.

### 2.3 Purification of MWCNTs

A typical purification procedure, [44] including oxidation in air, washing in 37% HCl acid (Sigma-Aldrich, ACS reagent) and, subsequently, rinsing by de-ionized and purified water (Milli-Q<sup>®</sup> Ultrapure WaterSystem), filtration and drying, was introduced for non-MWCNT, as described in Table 2.2.

Table 2.2: Purification procedure for non-MWCNT.

Step	Procedure	Notes
1	Oxidation: The oxidation temperature is 460 °C for 2 h. It is important that the metallic catalysis is oxidized thoroughly. Make sure that the MWCNT sample has good contact with air all the time, i.e. move the sample around every hour.	Oxidize metallic catalysis at high temperature. The sample is carried by a glass test tube. The oven has two heaters underneath a ceramic chamber.
2	Acid etching: The acid etching is taken place in a round bottom flask with magnetic stir, refluxed at 60 °C for 12 h.	Dissolve metal oxidant in HCl acid.
3	Rinse and dry: The MWCNT-HCl mixture was filtrated, subsequently rinsed with de-ionized water, and dried at 40 °C overnight.	The filtration process is carried out by a vacuum funnel system (Sigma-Aldrich, 47 mm), with Millipore <sup>®</sup> Isopore <sup>®</sup> , 0.6 $\mu\text{m}$ , polycarbonate, hydrophilic filter. Rinse sample until the pH of MWCNT-water mixture is 7.

<sup>2</sup> also denoted as F-MWCNT in Paper II, III and VI  
<sup>3</sup> denoted the same in Paper II and III

## 3. Buckminsterfullerene

### 3.1 A short history

$C_{60}$  (Figure 3.1) is a member in the fullerene family and was first discovered by Smalley and his colleagues in 1980s. [6, 45] It is composed entirely of carbon atoms forming a hollow spherical, football-like, structure. The molecule has 12 pentagonal and 20 hexagonal faces showing an icosahedra symmetry structure. Due to its small size with a van der Waals diameter of ca. 1.01 nm,  $C_{60}$  has been studied intensively for using as pure or hybrid material in the field of nanoscience and nanotechnology. [45] Table 3.1 provides the dimensions of the  $C_{60}$  molecule and a few important physical properties.

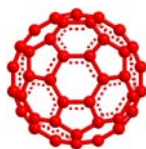


Figure 3.1: Schematic plot of a  $C_{60}$  molecule.

Table 3.1: Some distinct properties of  $C_{60}$ . [46]

Property	Number
Average C-C distance	0.144 nm
C-C bond length on a pentagon	0.146 nm
C=C bond length on a hexagon	0.140 nm
$C_{60}$ mean inner diameter	0.710 nm
$C_{60}$ outer diameter	1.034 nm
Density	1.72 g cm <sup>-3</sup>
Electrical conductivity	1×10 <sup>-14</sup> S m <sup>-1</sup>
Thermal conductivity	0.4 W m <sup>-1</sup> K <sup>-1</sup>
<sup>13</sup> C NMR chemical shift	143 ppm

$C_{60}$  is a potentially reactive molecule due to the many double bonds in its structure. These provide sites for bonds with other types of molecules or in between  $C_{60}$  molecules. In the latter case, two double bonds in two neighboring  $C_{60}$  molecules take part in a [2+2] cycloaddition mechanism, which gives covalent bonds between two  $C_{60}$  units. The process, which is initiated by visible or ultraviolet light, or treatment under HP&HT conditions, proceeds by reactions with other neighbors and gives a polymer-

like structure. This polymerization process gives orthorhombic, tetragonal or rhombohedral phases under high pressure conditions (Figure 3.2), as described by the phase diagram shown in Figure 3.3. At 1.5 GPa and a temperature of ca. 500 K, as used in this work, the  $C_{60}$  molecules polymerize into a mixture of orthorhombic and tetragonal structures, [47] as labeled in Figure 3.3.

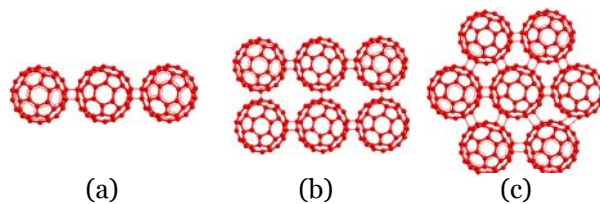


Figure 3.2: Polymeric structures of  $C_{60}$ : (a) orthorhombic lattice, (b) tetragonal lattice, (c) rhombohedral lattice.

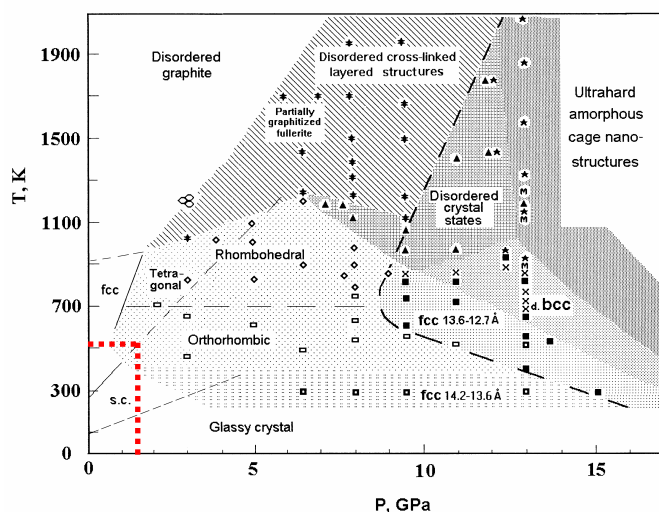


Figure 3.3: Phase diagram of  $C_{60}$  mapped under different pressure and temperature conditions, adapted from V D Blank et al., Carbon 36, 319 (1998). [48] The dotted lines indicate  $p$ - $T$  conditions used in this thesis work.

### 3.2 Specification of $C_{60}$ in this research

$C_{60}$  produced by chromatography and sublimed to remove solvents and other contaminants was purchased from MER Corporation, USA. The product is a black crystalline powder with a density of  $\sim 0.8 \text{ g cm}^{-3}$ . It has a stated purity of 99.9% with traces of  $C_{70}$  and  $C_{60}$  oxide as the main impurities.

## 4. The polymers and composite material

A polymer<sup>4</sup> is a large molecule (macromolecule) composed of a large number of identical structural units called constitutional repeating units. These subunits typically consist of carbon atoms and are connected by covalent chemical bonds. The properties of polymers do not vary markedly with the number of repeating units. [49] Because of low cost, ease of processability and a wide range of properties, polymeric materials play an essential and ubiquitous role in our everyday life. Biopolymers such as nucleic acids and proteins are essential for life; naturally existing polymer such as shellac, amber, and rubber have been used for centuries. Synthetic polymers, like synthetic rubber, nylon, polyethylene (PE), polypropylene (PP), etc., are some of the most widely used materials because of their versatile properties. [50]

### 4.1 Nylon-6

Polyamides are a family of synthetic polymers in which molecules are linked together by amide groups. The most well-known member in this family is nylon, a generic name for linear polymers consisting of methylene sequences in between amide groups. Various nylons, e.g. nylon-6, nylon-6,6 or nylon-12 etc., are referred to by the number of carbon atoms in the constitutional repeating unit, such as nylon-6 with six carbons in the repeat unit:  $[\text{CO}-(\text{CH}_2)_5-\text{NH}]_n$ . Nylon-6 is one of the most important engineering thermoplastics and it is also commonly used as a matrix for composite materials. Nylon-6 exhibits a high-strength semicrystalline structure and has one of the best temperature stability and chemical resistance among all polymers. [51] Resistance to heat, oil, wear and abrasion has made nylon an alternative candidate material in applications such as tire cords, gears and bearings etc. [51]

Nylon-6 can exist in at least two crystalline modifications: a stable monoclinic structure,  $\alpha$  phase and a monoclinic or pseudo-hexagonal crystal structure,  $\gamma$  phase. [51] Slow cooling from the melt yields mainly the  $\alpha$  phase whereas rapid cooling and crystallization at lower temperatures yields increasing amounts of the  $\gamma$  phase, and the  $\gamma$  phase becomes the dominant phase when crystallization occurs at  $\sim 130$  °C and below. The phases may co-exist but the  $\gamma$  phase has been found less stable and can be converted to the  $\alpha$  phase e.g. by annealing slightly below the melting temperature (493 K) and/or under stress. [51, 52]

---

<sup>4</sup> 'polymer' is derived from Greek, means 'many' (poly) and 'part' (mer)

## 4.2 Polyisoprene (PI<sup>5</sup>) and Polybutadiene (PB<sup>6</sup>)

The name 'rubber' was first introduced by Joseph Priestley in 1770 to describe the material which could rub out lead pencil marks from a paper, but later it has become almost synonymous with an elastomer, i.e. a polymer which can be reversibly extended, in some cases several times longer than its own length. In 2005, about 21 million tons rubber were produced and about 42% was made from natural rubber. The three largest producing countries are Thailand, Indonesia and Malaysia. [53]

The purified form of natural rubber (from latex) is PI (mostly *cis* 1,4 PI), which can be produced synthetically as well. The vulcanization of PI, i.e. the process of cross-linking between polymer chains with the aid of sulfur, improves the mechanical strength, elasticity of PI and reduces its sensitivity to changes in temperature. [54, 55] The viscoelastic and heat resistance properties of polymers are dependent on the type of cross-link, e.g. C-S-C or C-C, and cross-link density. During the vulcanization process, it is common to apply slight pressure to shape samples as well as to improve their mechanical properties.

PI is a pressure cross-linkable polymer, which means that the polymer can be cross-linked by a suitable combination of pressure and temperature conditions without the use of any chemical agent. [56] This opens a new way to study the properties of cross-linked material and cross-linking mechanisms.

As a member of the synthetic rubber family, PB is a polymer obtained by polymerization of the monomer 1,3-butadiene, and the process gives three different configurations: (vinyl) 1,2-, *cis*-1,4- and *trans*-1,4-PB. PB has a high resistance to wear and it is used especially in the manufacture of tires, which consumes about 70% of the production. [57]

PB is also possible to cross-link under high pressure. [58, 59] In fact, PB is much more reactive than PI, which means that it achieves a significantly higher cross-link density than PI after identical treatments. Among the three configurations, the pendant vinyl group is most reactive, which is one of the reasons for PB's higher tendency for cross-linking. In paper VIII, LPB and sPB were selected as matrixes to produce and study CNT filled polymers with very high cross-link density.

---

<sup>5</sup> Here "PI" refers to polyisoprene in general and not a specific  $M_w$  as in Paper IV, V, VI and IX

<sup>6</sup> Here "PB" refers to polybutadiene in general and not a specific  $M_w$  as in Paper VII and VIII.

### 4.3 The CNT based composite material: achievement and challenge

A composite material is an engineered or a naturally occurring material made from two or more constituent materials, with significantly different physical or chemical properties, which remains separated and distinct at a macroscopic or microscopic scale within the finished structure. [60] Composites make up a broad and important class of engineering materials. The annual production is over 10 M tons all over the world and increases ca. 5-10% every year. [61] For composites used as engineering materials, it is common to reinforce weak and soft matrixes with strong and stiff fibers or fillers, such as carbon black, silica, zeolites etc. [62] The objective is normally to obtain a strong low-weight material by inserting small amount of a strong and stiff component in a low-density matrix. Commercial material commonly has glass or carbon fibers in matrices based on thermosetting polymers, such as epoxy or polyester resins. For economical reasons, thermoplastic<sup>7</sup> polymers are preferred as matrix since they are re-moldable after initial production, which is not the case for thermosets<sup>8</sup>. There are also other classes of composites with metallic or ceramic materials as matrix, but these are not discussed here.

CNTs are, in theory, perfect for use as advanced fillers for manufacturing nanocomposite materials. As mentioned earlier, CNT is known as the strongest material. Besides, CNTs have the advantages of small diameter, large aspect ratio and low density, which are ideal for composite systems. According to the classical Halpin-Tsai equations, [40]  $\sigma_{UTS}$  and  $E$  of a composite can be estimated by:

$$\sigma_{UTS} = (\sigma_{filler} - \sigma_{PI}) \cdot V_{filler} + \sigma_{PI} \quad (4.1)$$

$$E = (E_{filler} - E_{PI}) \cdot V_{filler} + E_{PI} \quad (4.2)$$

where  $\sigma_{filler}$  and  $\sigma_{PI}$  are the  $\sigma$  of filler and PI, respectively;  $E_{filler}$  and  $E_{PI}$  are the  $E$  of filler and PI, respectively; and  $V_{filler}$  is the volume fraction of filler.

These equations suggest that even small amount of CNT fillers can very much increase  $\sigma_{UTS}$  and  $E$  of a composite. For example, the equations predict that 1 wt% CNT fillers may increase a composite's  $\sigma_{UTS}$  or  $E$  to ~10 GPa because both  $\sigma_{filler}$  and  $E_{filler}$  are very high (~ 1 TPa). However, experiments show much weaker reinforcement than that suggested by these equations.

A few studies concerning tensile reinforcement of CNT/polymer composite have been reported [63] where CNTs were either covalently bonded or non-covalently bonded to a polymer. For a bulk composite (or film) sample, an addition of 8.3 wt% MWCNT in nature rubber showed

---

<sup>7</sup> Thermoplastic is a polymer having a melting point.

<sup>8</sup> Thermoset is a polymer without melting point, which can only be cured once.

~900% higher  $E$  and ~60% higher  $\sigma_{UTS}$  than the pure polymer. [64] Even through the relative improvement was very good but since rubber is a soft material at the beginning, the resulting composite was still rather soft ( $\sigma_{UTS}=7$  MPa and  $E=10$  MPa).

The behavior of reinforced polymer fibers is slightly different (diameter ca. 100  $\mu\text{m}$ ). Fibers can reach relatively high  $\sigma_{UTS}$  and  $E$ , and particularly in cases of a rather hard matrix such as PMMA, [65] nylon, [66] epoxy, [67] and poly(vinyl alcohol) [68] etc. Moniruzzaman et al. [66] produced fibers of nylon 6, 10 and 1 wt% alkyl acid chloride group functionalized SWCNTs (SWCNT-(CH<sub>2</sub>)<sub>n</sub>-COCl), which showed over 2 times higher  $\sigma_{UTS}$  than fibers of nylon 6, 10 and 1 wt% non-functionalized SWCNTs. The results imply that covalent bonds between the nylon matrix and the functionalized CNTs increased the reinforcement. However, in many other cases, CNT/polymer composites do not show much improved strength and improvements are typically far from that predicted based on the extraordinary strength of CNT fillers. The reason is most likely due to weak CNT-polymer interfacial contact even though CNTs appear to be coated/warped by polymer chains. As a consequence, composites likely fail due to CNT pull-out as CNTs slip in the polymer matrix, and this limits the performance of CNT/polymer composites. In this thesis work, HP&HT treatment was introduced to study the changes in CNT-polymer interfacial contact. In particular, the properties of HP&HT treated bulk composites have been studied and the effect of HP&HT cross-linking was established.

Besides poor mechanical strength, it is well-known that polymers are relatively bad thermal conductors. The  $\kappa$  of polymers is typically in the range from ~0.1 to 0.6 W m<sup>-1</sup> K<sup>-1</sup>, [69] which is several order less than that of CNTs. As discussed in Chapter. 2, experiments show that  $\kappa$  of CNTs can reach as high as~ 3000 W m<sup>-1</sup> K<sup>-1</sup>. Thus, adding relatively small amount of CNTs may dramatically improve the heat transport in poor thermal conductors such as polymers. Especially since their high aspect ratio promotes percolation<sup>9</sup> at low mass fractions. Their large specific surface area should also be beneficial for the thermal contact with a polymer matrix. Strong improvements of  $\kappa$  has also been reported, e.g. Haggemueller et al. [70] found 600% increase of  $\kappa$  by adding 20 vol% SWCNTs in high-density PE. However, it is still significantly less than that suggested by a simple mixture rule:

$$\kappa_{Com} = \kappa_{polymer} + \kappa_{CNTs} \cdot f / 3 \quad (4.3)$$

where  $\kappa_{Com}$ ,  $\kappa_{polymer}$  and  $\kappa_{CNTs}$  are  $\kappa$  of composite, polymer and CNTs respectively and  $f$  is the volume fraction of CNTs. It predicts that a composite with ca. 1 wt% filler should achieve  $\kappa$  as high as ~10 W m<sup>-1</sup> K<sup>-1</sup> and that the increase observed by Haggemueller et al. [70] should have been ~39900%. The reason for this discrepancy is probably due to very high interfacial

---

<sup>9</sup> The capability of CNTs to form a nanoscale network structure

thermal resistance between the CNTs and the polymer matrix, [71-73] which arises from the mismatch of phonon modes in CNTs and polymers. In fact, Huxtable et al. [74] detected a very large interface thermal resistance across a CNT–sodium dodecyl sulfate (SDS) interface. Molecular dynamics (MD) simulations [74] showed that the high-frequency phonon modes in the CNTs must first be transferred to the low-frequency modes through phonon–phonon coupling before it can be exchanged with the surrounding medium (SDS here) as the surrounding of CNTs are coupled by a small number of low-frequency vibrational modes.

In this work, HP&HT treatment was applied to investigate the effects of cross-linking and crystallization of polymers on the interfacial thermal contact. Xu et al. [75] performed a simulation on the effect of engineering the CNT-polymer interface. They found that the large thermal resistance at CNT interfaces can be decreased significantly by tuning the wrapping density, resulting in larger overlap at low frequencies (below 70 THz). The modified molecular structure at the interface enhanced both the matching of phonon spectra and phonon mode coupling.

#### **4.4 Covalently bonded C<sub>60</sub>-PI composites**

For the purpose of studying dynamics between nanoparticle and polymer, many studies concerning C<sub>60</sub>-polymer composites were performed, [76-78] and showed that C<sub>60</sub> can elevate the glass transition temperature ( $T_g$ ) of polymers. [77] C<sub>60</sub> was proposed to reduce polymer segmental mobility in the vicinity of the particle surface and ultimately suppress polymer dynamics. [77] There are, however, relatively few investigations concerning tensile reinforcement of polymers by C<sub>60</sub> fillers, and these typically show that the tensile properties of C<sub>60</sub>-polymer composites are roughly the same as the neat polymer. [79]

In this thesis, it is shown that C<sub>60</sub> was most likely covalently bonded to PI after HP&HT treatment. The cross-linked microstructure showed significantly improved tensile properties. In addition, C<sub>60</sub> clusters behaved as reversible cross-linkers in the composite system. This is an interesting property and suggests that C<sub>60</sub>, or similar carbon nanofillers, can be used to design strong polymer materials, which can be recycled.

## 5. Sample synthesis and preparation

The key to obtain nano-composites with optimum properties is to homogeneously and uniformly disperse the nanoparticles inside the matrix. The CNT filled polymer composites studied in this work were prepared via either *in-situ* polymerization or solvent mixing, which are two methods that normally give good results.

### 5.1 *In-situ* polymerization

The *in-situ* polymerization starts with well mixed CNTs with monomer, followed by polymerization of monomers in the presence of CNTs. [13] Except generally well dispersed CNTs in the polymer matrix, *in-situ* polymerization facilitates the possibility of covalent bonding between functionalized CNTs and polymer. [13] In Paper II and III, a MWCNT/nylon-6 composite was synthesized via *in-situ* polymerization, which followed the steps suggested by Gao et al.[80, 81]: P-MWCNTs or MWCNT-COOH were first mixed with  $\epsilon$ -caprolactam (Aldrich, 99%) with an ultrasonic bath (35 kHz, Bandelin Sonorex® RK 52H) followed by sonication with ultrasonic pin at 80 °C. Subsequently, 1 g (10 wt% of  $\epsilon$ -caprolactam) 6-aminocaproic acid (Sigma,  $\geq 99\%$ ) was added to the suspension and the flask was transferred to a pre-heated silicon oil bath kept at 100 °C. The suspension was heated to 250 °C with mechanical stirring under dry nitrogen atmosphere and kept under these conditions for 6 h before cooling to room temperature. The cooled sample was transferred to a nitrogen filled bag and spooned out after slight heating. In order to remove un-reacted monomers and low molecular weight oligomers, the collected sample was cleaned by ultrasonic bath in water at 80 °C for 1 hour. Finally, the washed sample was dried by vacuum pumping at 80 °C for 48 h. A control sample of nylon-6 without MWCNT was synthesized using a similar procedure as for the composite:  $\epsilon$ -caprolactam and 6-aminocaproic acid were loaded into a three-neck round-bottom flask for polymerization.

### 5.2 Solvent mixing

Solvent mixing or solution blending is the most common and convenient route to prepare CNT/polymer composites. In general, it includes 3 major steps: i) disperse the CNT homogeneously in a suitable solvent which can also dissolve the polymer matrix; ii) dissolve polymer in this solvent separately and later mix the 2 mono-component solutions together to obtain a homogeneously distributed CNT/polymer mixture; iii) remove the solvent in

order to extract composite material. Practically, the CNTs, SWCNTs or MWCNTs, were dispersed in toluene (Thermo Fisher Scientific Inc., analytical grade) by a ratio of ca. 5mg: 1ml and dispersed using an ultrasonic pin for 1 h. Subsequently, PI with  $M_r$  of 38 000 (sPI), PI with  $M_w$  of 800 000 (LPI<sup>10</sup>), PB with  $M_r$  of 2600 (sPB) or with  $M_r$  of 100 000 (LPB) was added to the dispersed CNT-toluene mixture and further sonicated for 2 h in a partly sealed beaker. During the last hour of sonication, an air tube was inserted to assist the evaporation of the solvent and increase the viscosity of the CNT-polymer mixture. Finally, the highly viscous mixture was pumped in a vacuum oven for at least 48 h at 45 °C in order to remove all the remaining toluene.

### **5.3 Sample preparation**

#### **5.3.1 Hot press**

Some of the as-made composites needed further treatment to enable the studies of their properties. For *in-situ* hot-wire measurement, the liquid or liquid based composites (high viscous, paste like samples) could be loaded directly into the cylindrically shaped Teflon® sample cell, but the solid composites, which were in the form of irregular pieces could not. These were cast into plates by first melting in a piston-cylinder device (Figure 5.1), which was heated in a vacuum oven, and subsequently pressing with a load of 11 tons (ca. 90 MPa) for 20 min. The LPB and LPB based composite were produced by this procedure by melting at 120 °C. In the case of the nylon-6 and nylon-6 based composites, which absorbs water and react with oxygen at high temperatures, the melting of the samples were done in a glove box with Ar atmosphere at 250 °C, and the samples were formed to plates by pressing the top piston of the piston-cylinder device by hand.

---

<sup>10</sup> LPI needs to be dissolved first in toluene

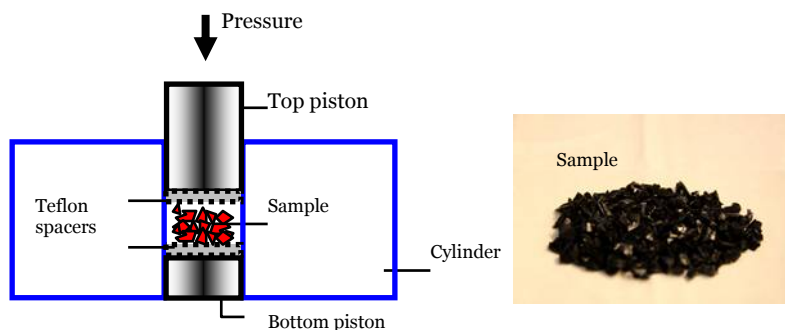


Figure 5.1 Hot-press cylinder (left) and synthesized CNT-polymer composite (right).

### 5.3.2 Spin coating

Spin coating is a widely adopted method to produce thin film samples on a flat substrate. Briefly, an excess amount of solution is injected on the substrate, which is rotated at high speed in order to spread the fluid by centrifugal force forming thin film. [82] For the purpose of preparing a thin film sample which could be HP&HT treated and recovered afterwards, an aluminum and stainless steel substrate (diameter of 39mm as inner diameter of Teflon® cell) were designed. A typical procedure is described in Table 5.1

Table 5.1: Spin coating procedure.

Procedure	Description
1. Stage 1:	5 s spinning at 600 rpm
2. Stage 2:	15 s spinning at 1000 rpm
3. Baking of sample	80 °C at hot plate for 3 min
4. repeat procedure 1-3 3 times	Obtaining thicker film

## 6. *In-situ* sample characterization

### 6.1 High pressure equipments and their functions

#### 6.1.1 Press family

The high pressure studies in this thesis were done using the blue and yellow presses (Figure 6. 1), with 1500 ton and 200 ton load capacities, respectively. The yellow press was used for studies up to its maximum capacity of 1.0 GPa, and the blue press was used for treatments in the 1-1.7 GPa range. The pressure generated by the hydraulic presses was calculated from load/area with an empirical correction for friction, which had been established using the pressure dependence of a Manganin wire. [83] The maximum pressure inaccuracy was estimated as  $\pm 40$  MPa at 1 GPa, but the pressure gradient in the probed sample volume, which is within a few mm from the hot-wire, is significantly smaller. [84, 85] During the isobaric runs, the pressure was kept constant to within  $\pm 1$  MPa using proportional–integral–derivative (PID) controller.



Figure 6.1: Image of presses in Experimental hall in Dept. of Physics, Umeå University (from left to right: blue, green, yellow, red and violet).

#### 6.1.2 Piston-cylinder apparatus and Teflon® cells

A piston-cylinder setup together with custom-made Teflon® sample cells were used in this work (Figure 6.2). The pressure on the sample was generated by forcing the top piston into the cylinder device. The temperature of the sample was measured by a chromel-alumel thermocouple (type K) placed in between sample plates or immersed in a liquid sample. The thermocouple had previously been calibrated to within  $\pm 0.2$  K of a commercially calibrated diode sensor, which has an accuracy of 10 mK.

During the annealing process, the temperature was controlled by another PID controller and kept constant to within  $\pm 1$  K. Another thermocouple, placed in the bottom of the Teflon<sup>®</sup> cell, was occasionally used for differential thermal analysis (see Section 6.3). For some sensitive samples, such as nylon-6 and MWCNT/nylon-6 composites, the Teflon<sup>®</sup> cell was assembled under dry argon gas to avoid moisture and oxygen, which may cause reactions at high temperatures. The Teflon<sup>®</sup> cell (Figure 6.2), which contained the sample, was used for hot-wire measurement, differential thermal analysis or temperature monitoring. It was subsequently transferred into the piston-cylinder apparatus (Figure 6.3). The cylinder could be heated to  $\sim 540$  K by an external heater or cooled to low temperatures ( $\sim 100$  K) by spraying liquid nitrogen.

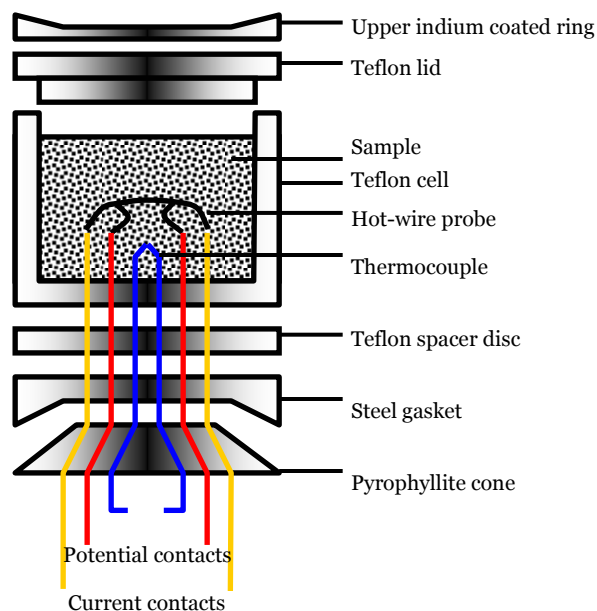


Figure 6.2: The separate parts of a typical hot-wire Teflon<sup>®</sup> cell.

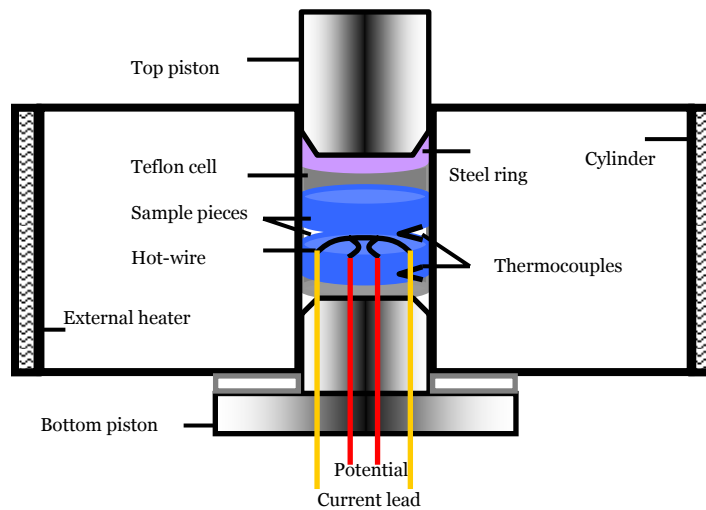


Figure 6.3: A schematic plot of an assembled piston-cylinder system with hot-wire and differential thermal analysis function Teflon® cell.

### 6.1.3 Support electronics and program

Software programs were designed for automatic reading and processing of data. Voltmeters were used to record temperature and pressure readings, which were converted to temperature in K and pressure in GPa by previously established calibration functions. The key features of the programs are to trig the measurement as a function of pre-set temperature, pressure or time steps and store the data after measurements. The programs used for various applications are listed in Table 6.1.

Table 6.1: Description of programs for certain measurements.

Application	Program	Main feature
<i>In-situ</i> hot-wire measurement	Visual C++	Measuring $\kappa$ and $\rho c_p$
<i>In-situ</i> differential thermal analysis	Labview®	Measuring $\Delta T$
<i>In-situ</i> impedance measurement	Labview®	Measuring Resistance, capacitance

### 6.2 *In-situ* transient hot-wire measurement

*In-situ* hot-wire measurement can measure  $\kappa$  and  $\rho c_p$  simultaneously under HP&HT conditions. The method is also an important tool to detect phase transitions, cross-linking and crystallization in materials.

### 6.2.1 A brief introduction to thermal conductivity $\kappa$

The  $\kappa$  is the property which shows a material's ability to conduct heat. The  $\kappa$  of a solid is defined by Fourier's law in one dimension: [86]

$$j_U = -\kappa \frac{dT}{dx} \quad (6.1)$$

where  $j_U$  is the energy transmitted across unit area per unit time,  $dT/dx$  is the temperature gradient. In a simplified description, the energy is carried by quasiparticles, phonons, which encounter frequent collisions. Based on this simplified view, it is possible to derive the Debye model for  $\kappa$  as:

$$\kappa = 1/3 \cdot C \cdot v \cdot \ell \quad (6.2)$$

where  $C$  is the heat capacity of phonons,  $v$  is the phonon velocity, and  $\ell$  is the phonon mean free path. In this equation,  $\ell$  is the most dominate factor. If the propagation of phonons in a lattice is purely harmonic, then the mean free path is only limited by collisions of phonon at crystal boundaries and lattice imperfections, impurities etc. However, in a real lattice, anharmonicity causes also phonon-phonon scattering.

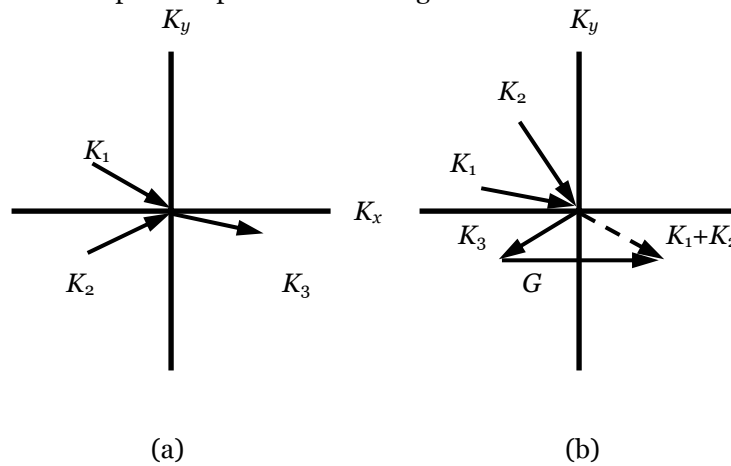


Figure 6.4: Phonon collision processes in a two dimensional square lattice: (a) normal mode and (b) Umklapp processes. [86]

There are various types of phonon scattering, e.g. phonon-phonon scattering and phonon-structural scattering. In the former interaction, phonons can be created or destroyed subjected to momentum and energy conservation. Assuming an interaction involving three phonons, where two

combine into one, this can be express in terms of the wave vectors  $K$  as (Figure 6.4a):

$$K_1 + K_2 = K_3 \quad (6.3)$$

which is referred to as a normal process. A normal process does not directly cause thermal resistivity since the heat current carried by the two phonons that combine into a new continues in the same direction after the process. The most important three-phonon processes that directly cause thermal resistivity are referred to as Umklapp processes (Figure 6.4b). In this case the combined wave vector is outside the first Brillouin zone and is therefore reflected back into the first zone by a reciprocal lattice vector  $G$ , which is described by:

$$K_1 + K_2 = K_3 + G \quad (6.4)$$

This phonon process contributes directly to the thermal resistivity since the heat current carried by the merged phonons now moves in an almost reversed direction.

### 6.2.2 Transient hot-wire method: the theory

The transient hot-wire measurement is based on the exact solution for the temperature rise  $\Delta T$  of an infinitely long, straight, infinitely conducting wire in an infinitely large specimen, as previously stated by Håkansson et al. [87]:

$$\Delta T = T(t) - T_0 = \frac{2q\alpha^2}{\pi^3 \kappa} \int_0^\infty \frac{1 - \exp(-\tau \cdot u^2)}{u^3 \Delta(u, \alpha)} du \quad (6.5)$$

where  $q$  is the constant heating power per unit length (of the wire),  $\kappa$  is the thermal conductivity of specimen,

$$\Delta(u, \alpha) = (uJ_0(u) - \alpha J_1(u))^2 + (uY_0 - \alpha Y_1(u))^2 \quad (6.6)$$

where  $\Delta u$  is the combination of Bessel functions, in which  $J_0$ ,  $J_1$  are Bessel function of the first kind of zeroth and first order, whereas  $Y_0$ ,  $Y_1$  are Bessel function of the second kind of zeroth and first order.

$$\alpha = \frac{2\rho c_p}{\rho_w c_w} \quad (6.7)$$

where  $\rho$  and  $\rho_w$  are the density of specimen and wire respectively,  $c_p$  and  $c_w$  are the heat capacity of specimen and wire respectively,

$$\tau = \frac{\kappa \cdot t}{\rho c_p r^2} \quad (6.8)$$

where  $t$  is time, and  $r$  is the radius of the wire.

This solution, given by Carslaw and Jaeger, [88] is based on the following ideal conditions: (i) the hot-wire with a radius  $r$  is infinitely long, has a heat capacity of  $c_w$ , density of  $\rho_w$  and an infinite  $\kappa$ ; (ii) the temperature of hot-wire

and specimen at time  $t=0$  is  $T_0$ ; (iii) at  $t=0$ , the hot-wire is heated by a uniform power per unit length  $q$ .

In order to get the experimental values of  $\kappa$  and  $\rho c_p$ , the relation between temperature rise ( $\Delta T$ ) as a function of  $t$  needs to be established with a known  $q$ ,  $\rho_w$ ,  $c_w$  and  $r$ .

### 6.2.3 Experimental setup of hot-wire measurement

The hot-wire measurements are performed in a Teflon® cell with a hot-wire probe made of nickel (Figure 6.5). [89] Nickel has a strong temperature dependent resistance and a fairly good mechanical strength under elevated pressure and temperature conditions. It is therefore well suited for hot-wire measurements. The hot-wire length, i.e. the length between the potential contacts, is about 40 mm. It is measured accurately ( $\pm 0.01$  mm) by a Nikon workshop microscope before it is soldered with copper contacts, which further connects to an external circuit. The diameter of the hot-wire could be either 0.1 or 0.3 mm where the potential lead is always 0.1 mm. One thermocouple is located in the sample and, occasionally, a second one is inserted close to the wall of the cell for use in differential thermal analysis. In the case of a solid sample, it is normally melt-cast into two sample plates and the hot-wire probe is sandwiched in between. For liquid or highly-viscous samples, it is more convenient to simply pour or spoon the sample into the cell.

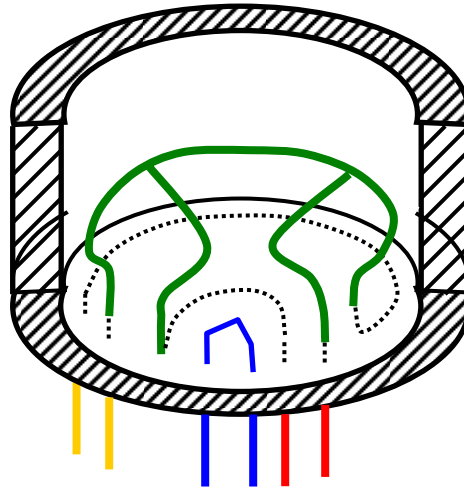


Figure 6.5: A typical sample cell arrangement with the hot-wire probe soldered onto copper wires in a Teflon® cell.

The hot-wire probe is connected externally to an electronic circuit, which is in charge of triggering of heating pulse, the intensity of pulse etc. The circuit is described in detail in previous publications and is therefore only schematically described here (Figure 6.6). [87, 90, 91] In a typical measurement sequence (Figure 6.7), the electronics trigger a 1.4 s long electric pulse of almost constant power, which is fed through a manganin wire and the hot-wire probe. The power is set to rise the sample temperature by about 3.5 K, and it is measured via the voltage of the manganin wire (voltmeter 2), which has a temperature-independent, known, resistance. To determine  $\kappa$  and  $\rho c_p$ , the hot-wire's resistance (in total 29 points,  $R_1$  to  $R_{29}$ ) is measured as a function of time (corresponding to the times  $t_1$  to  $t_{29}$ ), by voltmeter 1. The temperature rise of the wire is then determined by its electrical resistance-temperature relation, i.e., the wire acts as both heater and sensor for the temperature rise. Measurements sequences can be initiated automatically as a function of temperature (isobaric runs), pressure (isothermal runs), and time. The latter is used to study, e.g., sluggish cross-linking or crystallization processes of materials as a function of time while the pressure and temperature are kept constant.

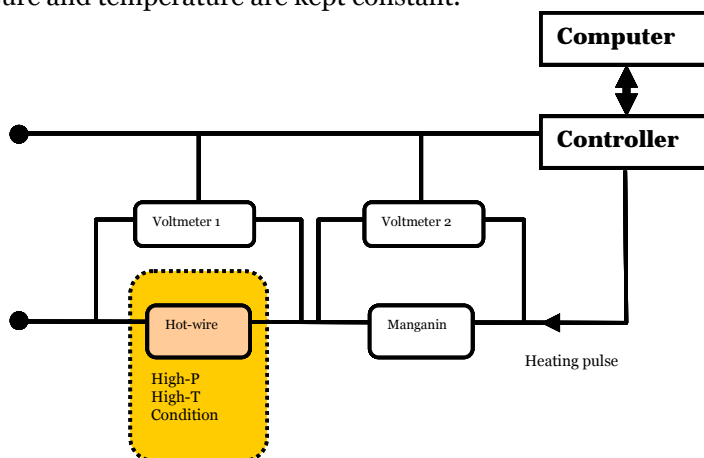


Figure 6.6: Simplified hot-wire measurement circuit.

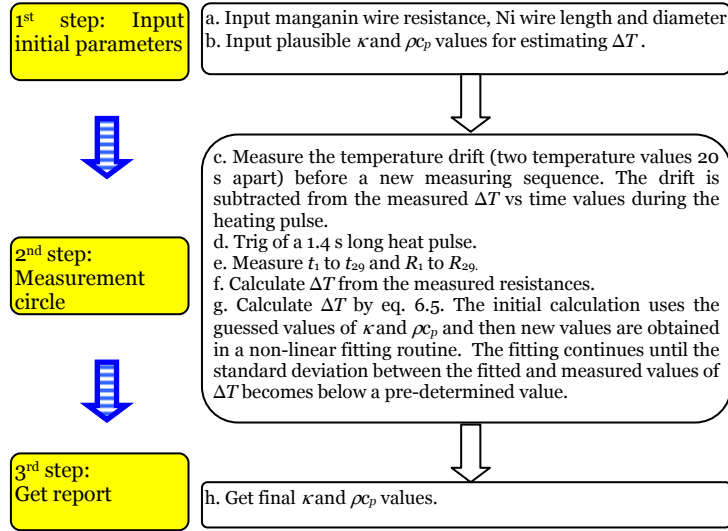


Figure 6.7: A hot-wire measurement sequence.

### 6.2.4 The details of calculation of $\kappa$ and $\rho_p$

As described above, one needs to establish the relationship between the hot-wire's temperature rise ( $\Delta T$ ) and time ( $t$ ) from measured values of its resistance versus time. The resistance of nickel is very sensitive to temperature, and the resistance-temperature relation ( $f(T)$ ) was determined separately in a calibration experiment, as described by Andersson. [90] Therefore, the resistance of the hot-wire is given by:

$$R_{\text{hot-wire}}(T) = R_s f(T) \quad (6.9)$$

where  $R_s$  is the initial resistance of hot-wire and  $f(T)$  is the temperature dependence function of hot-wire.

If the start of the heating pulse is defined as time  $t_0=0$  then the first measured resistance is obtained at time  $t_1$  and is given by  $R_1$ . Similarly, all the measured 29 points of resistances correspond to certain times as:  $t_1$  to  $t_{29}$  and  $R_1$  to  $R_{29}$ . Comparing the  $R$  before the start of the pulse ( $R_0$ ) with one of any other ( $R_i$ ):

$$\frac{R_i}{R_0} = \frac{f(T_i)}{f(T_0)} \quad (6.10)$$

therefore the temperature rise by the heating pulse could be expressed as:

$$T_i = \frac{f^{-1}(R_i \cdot f(T_0))}{R_0} \quad (6.11)$$

At one measurement, with  $R_1$  and  $T_0$  obtained from measurements, together with  $T_1=T_0+\Delta T$ , ( $\Delta T$  is first obtained approximately by making a plausible estimate of  $\kappa$  and  $\rho c_p$ )  $R_0$  can be determined by eq. 6.11. When  $T_0$  and  $R_0$  are known, all the measured  $R_i$  values can be converted to  $T_i$  values via eq. 6.11. An analytical solution is fitted to these 29 data points in a non-linear fitting routine until the change in  $\kappa$  is less than 0.1% and the change in  $\rho c_p$  is less than 0.5% compared to the preceding values obtained by eq. 6.5. Because the calculation of eq. 6.5 is time consuming, values for  $\Delta T$  have been calculated in advance and are saved in a two-dimension table. (eq. 6.5 is an integral of two dimensions,  $\kappa$  and  $\rho c_p$  or the variables  $\tau$  and  $\alpha$  as defined in Section 6.2.2, which are the variables used in the table.) The inaccuracies are estimated as  $\pm 2\%$  in  $\kappa$  and  $\pm 5\%$  in  $\rho c_p$ .

### **6.3 *In-situ* differential thermal analysis**

Phase transformations such as melting, crystallization, or change in crystal structure are normally associated with absorption or release of heat. By placing one thermocouple in the sample and another in the Teflon® cell, e.g. underneath the sample, it is possible to detect phase transformations through the temperature difference caused by the heat absorption or release, which is measured by the two thermocouples. A program was therefore designed to simultaneously measure the temperature at these places typically every 30 s.

### **6.4 High-pressure high-temperature treatment**

High-pressure high-temperature treatment (referred to also as ‘HP&HT treatment’, ‘treatment’ or ‘treated’ in this thesis) consists of a series of changes in pressure, temperature together with an annealing step. At the beginning, the sample is isothermally pressurized from room temperature and atmospheric pressure to a certain pressure. This is followed by isobaric heating up to a high temperature, typically ~500 K. Subsequently, the sample is kept at this temperature for a long time (typically 4 h), i.e. the sample is annealed at constant pressure and temperature. During the annealing step, and under the conditions used here, the sample transforms slowly to a new state with a significantly different microstructure. After this step, the sample is cooled (isobarically) to room temperature and thereafter depressurized to atmospheric pressure and recovered. In contrast to pressurization cycling near room temperature, HP&HT treatment induced an irreversible (permanent) change of the samples due to chain scissoring, cross-linking or/and crystallization.

## 7. Tensile measurement

Mechanical properties such as the tensile strength ( $\sigma_{UTS}$ ), tensile strain or elongation at break ( $\epsilon_B$ ) and Young's modulus ( $E$ ) are key parameters for engineering/structure materials. These are measured in a tensile tester in which the sample is subjected to uniaxial tension at a constant rate until failure. In this thesis, CNT or  $C_{60}$  was added into polymers as reinforcement filler to study the effect on the tensile properties.

Figure 7.1 shows the typical stress-strain behavior of brittle, ductile and elastomeric materials. A hard, brittle material normally has a small  $\epsilon_B$  ( $\sim 10\%$ ), and large  $E$ . A ductile material has the ability to deform (irreversibly) under tensile stress, which occurs after the yield point (point d in the Figure 7.1). A typical elastomeric material shows long extension but small  $E$  since it is comparably soft. The points a, b, c, in Figure 7.1 are the  $\sigma_{UTS}$  of materials.

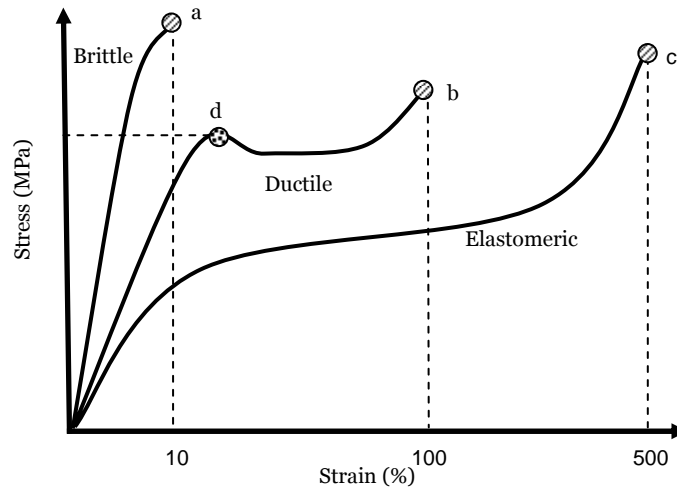


Figure 7.1: The stress-strain curves of some typical behaviors. [92]

### 7.1 Tensile properties of polymer based composite material

The importance of fiber filled composites arises from the flexibility of design and fabrication of the material with high strength and stiffness. As mentioned previously in Chapter. 4, the reinforcement of CNT filled polymers is much less than that predicted by the Halpin-Tsai model. There are many factors affecting the tensile performance of composites: the polymer properties such as cross-link density and crystallinity; CNT properties, e.g., aspect ratio, dispersion and alignment; as well as the

interaction between filler and matrix, i.e. covalent bonding, interfacial stress transfer etc. The failure of the theoretical model is most likely predominantly due to insufficient load transfer at the CNT-polymer interface, which can significantly limit  $\sigma_{UTS}$  and  $E$ .

Several efforts have been made to improve the interfacial contact. One method is to functionalize CNTs with side groups which provide sites for covalent bonds with polymer chains. This approach has shown good results at low concentration of CNTs (typically ca. 1 wt%) but it is difficult to achieve the same improvement with high CNT loading. [63, 66] Another possibility is to carefully design a reticulate architecture in order to optimize the molecular level couplings at the CNT-polymer interface. [67]

HP&HT treatment can enhance the physical interaction between CNTs and polymer, especially in a highly densified, cross-linked matrix. There is apparently an attractive interaction between CNTs and a polymer already without HP&HT treatment (see Paper VI), but it becomes much more significant after such treatment. This improved physical interaction means that the CNTs provide better reinforcement of a polymer matrix. This occurs simultaneously as a strong increase in the cross-link density measured by the swelling method ( $v_{Swell}$ , see section 8.9.1). The results of this work suggest that this increase is not due to significantly more chemical cross-links in the composites system than in the neat polymer but instead reflects the improved interfacial interaction. [93, 94]

## 7.2 Experimental setup

The tensile measurements were performed at room temperature (ca. 298 K) by an Instron 3343 tensile tester equipped with a 500 N or 1000 N load cell using a testing speed of 10 mm/min (Figure 7.2a). To ensure accuracy and repeatability, several pieces were commonly tested from the same sample (sometimes 3 pieces).

Two custom-made dog-bone shape dies (Die 1: 16mm in length×7mm in width; Die 2: 14mm in length×4mm in width, Figure 7.2b) were used to cut the HP&HT treated polymer/composite samples or hot-cast untreated samples into dogbone shape for tensile testing. The exact dimensions of samples were measured by means of a Nikon workshop microscope ( $\pm 0.01$  mm), and these values were used in the calculations of the tensile stress and  $E$  (in the range of 1-5% strain for brittle material such as HP&HT treated PI, MWCNT/PI).

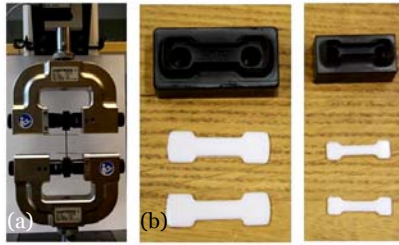


Figure 7.2: Images of (a) tensile tester; (b) Teflon® samples used for calibration and dies.

### 7.3 Repeatability and calibration of tensile tester

In order to investigate the repeatability of tests (based on 3 samples) as well as the effect of different sample dimensions on the tensile properties, Teflon® was used as testing material. All tests were done using the 1000 N load cell at room temperature (ca. 298 K) with a testing speed of 10 mm/min. A purchased Teflon® sheet (1.5 mm thick, from Plastica AB, Sweden) was cut by the dogbone shaped dies 1 and 2. The exact dimensions of the samples were measured by a Nikon workshop microscope and  $E$  was calculated in the range of 1-20%.

As depicted in Figure 7.3, the large dogbone showed average values for  $\sigma_{UTS}$ ,  $E$  and  $\epsilon_B$  of 31.6, 328 MPa and 410%, respectively, with a coefficient of variation<sup>11</sup> of 2.0%, 6.0% and 8.5%, respectively. The corresponding values for the small dogbone were 35.8 and 374.5 MPa and 374% with a coefficient of variation of 2.1%, 2.7% and 6.1%, respectively. The small dogbone showed slightly better reproducibility of the measurements. In general, the small dogbone showed higher  $\sigma_{UTS}$  (~14%) and  $E$  (~14%) than the big dogbone but  $\epsilon_B$  was shorter (~10%). With increasing dimension of the sample, the number of material defects and imperfections increases, which might explain the differences observed here.

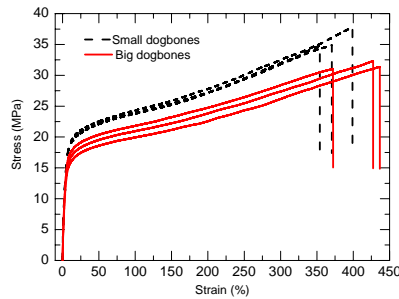


Figure 7.3: Stress-strain curves for dogbones with different dimensions.

<sup>11</sup> defined as standard deviation/average

## 8. Sample characterization

The distribution and orientation of the filler, and the morphology of the matrix are key parameters for the properties of composites. It is therefore essential to characterize the composite structure. The nano-size of the filler means that only the most powerful microscopic techniques can be applied to image the fillers and the composite samples, and these are summarized in Table 8.1.

Table 8.1: Comparison between atomic force microscope (AFM), scanning electron microscope (SEM), TEM and optical microscope (OM). [49, 95-97]

	OM	(HR-) SEM	(HR-) TEM	AFM
Resolution	0.2 $\mu\text{m}$	(0.4 nm) 4 nm	(0.08 nm) Sub-nano	Sub-nano
Objects	Surface, bulk	Surface	Surface, bulk	Surface
Radiation damage	None	Some	Severe	None
Specimen environment	Ambient	Vacuum	Vacuum	Ambient
Specimen preparation	Easy	Middle	Difficult	Middle
Daily maintain cost	Low	High	High	Middle

### 8.1 Atomic force microscope

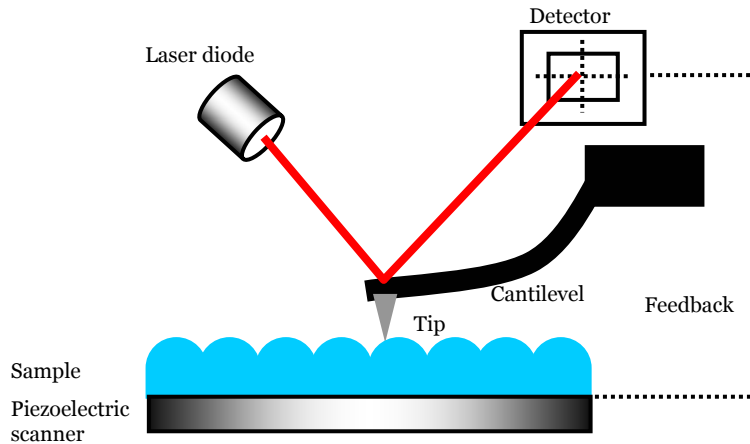


Figure 8.1: Schematic plot of a typical AFM setup.

AFM is one of the foremost tools for imaging, measuring, and manipulating matter by scanning the surface of a sample. Piezoelectric elements together with a laser system record movements accurately. The AFM probe holder

consists of a cantilever with a sharp tip (probe) where only the tip contacts the sample surface. A standard cantilever is usually made of silicon, with tip radius of a few to a few tens of nanometers (less than 50 nm). When the tip of the probe ‘scans’ the sample surface, the interaction between the tip and the sample results in a change in the feedback system, which is used to produce the image. Depending on the application, the measured interactions between the probe and the sample surface include mechanical contact force (contact mode), van der Waals force (tapping mode), capillary force, electrostatic force (electrostatic force microscopy, EFM), magnetic force (magnetic force microscopy, MFM), etc.

Table 8.2: Advantages and disadvantages of AFM.

Advantages	Disadvantages
<p>*Can measure under ambient condition No high vacuum chamber or electron gun is needed in this case, comparing to SEM and TEM.</p>	<p>* Low scan speed Compared to other electron microscopic techniques, which can image fair fast, a decent quality AFM image (3×3 μm<sup>2</sup>, resolution 1024×1024) normally take 30 min (scan rate 0.5 Hz).</p>
<p>*High resolution image This is of course limited by probe, but a LTESP probe with 8 nm tip radius can easily image a single SWCNT or MWCNT or polymer crystal spherulites.</p>	<p>*Fragile probe The silicon probe can be relatively easily damaged with a change in its properties e.g. sensitive to measuring parameters and sample conditions. The optimal using time is difficult to predict, and changing and calibration of new probes take extra time.</p>
<p>*Phase image function This feature can be used to easily distinguish two or more components in a material, like CNTs and polymers.</p>	<p>*Environment sensitive The ideal measuring condition would be dark, quiet room with a vibration-free table.</p>
<p>* 3-dimension profile AFM can provide a 3-dimensional profile of the sample surface, which is not possible with TEM.</p>	<p>*Limited scan size and height The scan size (1 dimension) is limited to a few hundred μm, and scan height is only a few μm.</p>

### **8.1.1 Contact mode AFM**

In the contact mode, the probe scans back and forward while being in direct contact with sample surface. The deflection of the probe causes a change in the reflected laser beam, which is detected by the detector (Figure 8.1) and used as a feedback signal. The force between the tip and the surface is kept constant during scanning by maintaining a constant deflection. The

deflection corresponds to a normal force which can be calculated by Hooke's law. [98]

Because the measurement of a static signal is sensitive to noise and drift, low stiffness cantilevers are used to enhance the deflection signal. However, close to the surface of the sample, attractive forces can be quite strong, causing the tip to "snap-in" to the surface, which can cause quite a damage to the sample. This effect gets more pronounced with decreased tip radius. Therefore, contact mode AFM is not suitable to investigate soft materials such as polymers.

### **8.1.2 Tapping mode AFM**

In ambient conditions, most samples develop a liquid meniscus layer. Tapping mode AFM is developed to keep the probe tip close enough to detect the short-range forces but long enough to prevent the tip from sticking to the surface.

In tapping mode, the oscillation of cantilever is driven near the resonance frequency of the cantilever by a piezoelectric element placed in the AFM probe holder. The amplitude of probe oscillation decreases when the probe is approaching to sample surface, due to the interaction such as van der Waals force, electrostatic force, etc. A piezoelectric actuator is used to control the height of the cantilever above the sample surface and maintain a set cantilever oscillation amplitude as the cantilever is scanned over the sample. A tapping mode AFM image is therefore produced by controlling the amplitude of the cantilever oscillation. [98, 99]

Since the probe does not contact sample surface directly during the measurement, the tapping mode is ideal for studying soft materials such as polymer, thin film material etc. and the mode also increases the lifetime of the probes compared to contact mode.

#### *\*Phase image*

In tapping mode, phase images are generated based on the phase lag between the oscillation frequency of cantilever and driver (the difference between the phase angle of the excitation signal and the deflection of the cantilever), [98, 100, 101] as shown schematically in Figure 8.2. The difference in phase angle could be applied for compositional mappings of composite material as well as to image material properties. [102] For example, Garcia and Tamayo [103] demonstrated by simulation that the phase signal in soft materials is sensitive to viscoelastic properties and adhesion forces, independent of elastic properties. In this thesis work, phase image of composite sample is very useful to distinguish filler and matrix material, evaluate the dispersion of filler in the polymer etc.

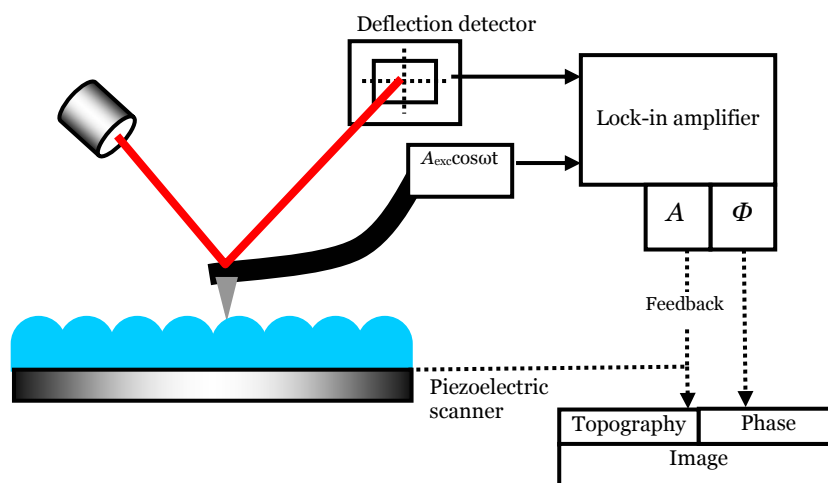


Figure 8.2: Instrumentation setup for phase image in tapping mode. The  $\Phi$  is the phase shift,  $A_{exc}$  is the excitation amplitude.  $A$  is the amplitude. [98]

### 8.1.3 Sample preparation

It is essential to have a flat sample surface prior to AFM measurements. For a 'hard' polymer composite sample, (e.g. 1.5 GPa treated MWCNT/sPI composite, 1.0 GPa treated MWCNT/nylon-6 composite and 1.5 GPa treated  $C_{60}$ /sPI composite), an ultramicrotome was used here for sample preparation. A blade, or an ordinary microtome, gives too many scratches and knife marks, which changes the surface morphology of a sample. Similar to the TEM sample preparation (Section 8.2.1), the sample was glued on an epoxy sample holder and cut by an ultramicrotome. But since the AFM only detect the sample surface, it does not require the same extreme sample thinness as TEM, which reduces experimental difficulties. According to my experimental experience, a semi-thin sample with thickness about 500 nm is excellent for sample scanning meanwhile the sample preparation procedure would not be very tedious.

For soft polymer composites (e.g. CNT/sPI composites treated at 1.0 GPa or below), it is possible to obtain decent sample quality by cutting the sample with a blade or microtome unless a quantitative comparison between samples are needed. [94] For a comparison of morphology of samples produced at different high pressure conditions, the sample preparation is more difficult. The ultramicrotome cannot be used since the sample will slip when the knife touches the soft surface. In most cases, the knife just

scratches at the surface leaving knife marks. In order to overcome the problem, a cryoultramicrotome (Leica EM FC 7) was applied.

Cryoultramicrotomy is a process of cutting ultrathin sections at low temperatures. It is widely used for biological samples as well as in material science. [104] The cutting of plastic and rubbery materials at low temperature avoids distortion of the microstructure and minimizes the stress after cutting. [104] The procedure used here was to glue the sample onto a metallic sample holder, which was cooled to ca. 100 K by liquid nitrogen before cutting. The setup allows continuous circulation of liquid nitrogen around a chamber, where the knife and sample are located. During the cutting, the temperature of the knife and sample was maintained at ca. 100 K by controlling the pumping of the liquid nitrogen. However, the cutting speed at these conditions is very slow and normally only a partially polished surface (~a few mm<sup>2</sup>) is obtained.

#### ***8.1.4 The probes and images***

The tapping mode or contact mode AFM was carried out by a MultiMode AFM (equipped Nanoscope IV Controller, Veeco Metrology). The selection of probe is another critical condition for the quality and resolution of image. Due to nano-scale feature of CNT, the probes (Veeco® probe or Bruker® probe) with small tip radius are preferred.

##### ***\*LTESP***

LTESP is a tapping-mode type, non-coated, etched silicon made probes, has a tip radius of 8 nm and force constant of 48 N/m operated at a resonant frequency of 190 KHz. This probe has a long cantilever (225 μm) with low resonant frequency. The small tip radius enables precise and high resolution image. This probe has best performance for imaging either CNT or polymer based composite material in this thesis.

##### ***\*RTESP***

RTESP is also a tapping-mode, non-coated, etched silicon probe, which has a tip radius of 8 nm and a force constant of 40 N/m, and it operates at a resonant frequency of 300 KHz. However, this probe is less stable than LTESP for the samples studied in this work.

##### ***\*MSNL***

MSNL is a probe with a 2 nm silicon tip on a silicon nitride cantilever, which has a low spring constant and high sensitivity. This super-sharp probe has

six cantilevers with force constant from 0.01-0.50 N/m and Au reflective coating. It can be operated in tapping mode and is suitable for any media (even liquid).

*\*OSCM*

This probe is designed for EFM mode. The platinum coating (20 nm) on the front side of the cantilever allows a metallic electrical path from the cantilever to the tip. This probe has a tip radius of 15 nm, operating at 2 N/m and 70 KHz. The Al coating on the back side (100 nm) of cantilevers compensates for the stress created by the front side coating and also enhances laser reflectivity (signal sum) by a factor of up to 2.5 times.

*\*Image artifacts*

As with other microscopic techniques, image artifacts such as distorted features and uneven morphology may arise. These kinds of artifacts can be caused by old/inappropriate probes, bad sample surface, and unsuitable operation parameters etc. Due to the fragileness of AFM probes, it is not recommended to measure steep walls or overhang features over 100 nm.

## **8.2 Transmission electron microscope**

TEM is a microscopy technique whereby a beam of electrons is transmitted through an ultra thin specimen, interacting with the specimen as passing through. An image is obtained from the undiffracted electrons transmitted through the specimen. In general, a region with high density scatters more electrons therefore with darker appearance than the region with low density with bright appearance. In this way the contrast of image is created. The final image is magnified and focused onto an imaging device (Figure 8.3a), such as a fluorescent screen or CCD camera. TEM is capable of imaging at very high resolution, and resolve items as small as a single column of atoms attached on the wall of a CNT.

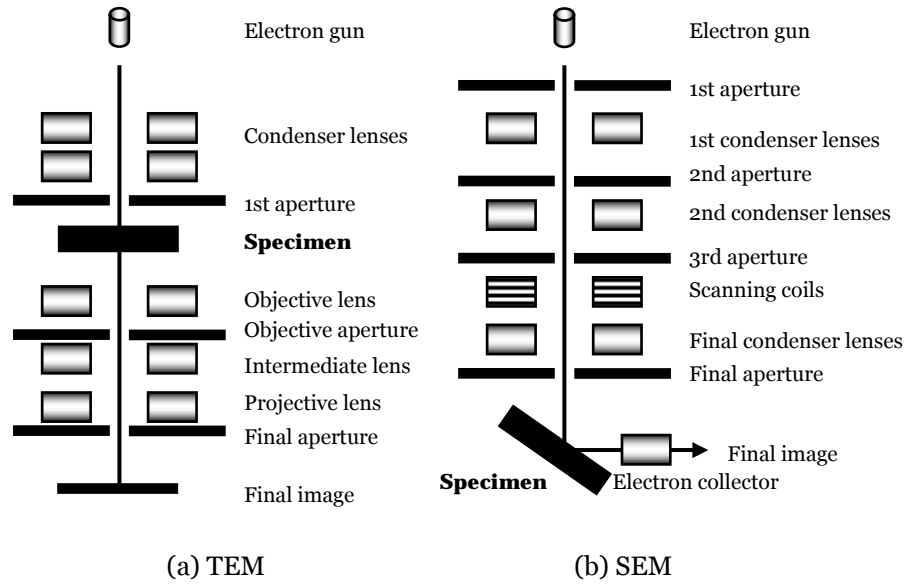


Figure 8.3: Schematic views of: (a) TEM and (b) SEM.

### 8.2.1 TEM sample preparation: ultramicrotome sectioning

A bulk polymer composite need to be sectioned into thin slices before observing by TEM since the electron beam cannot pass through a sample of more than 100 nm thickness. For observations by high-resolution TEM (HR-TEM), the sample thickness should be around 50 nm or even less. A typical specimen consists of several pieces of ultra-thin sections (50-80 nm) carried on a TEM grid (copper grid in this thesis). How to obtain thin sections is the key part for the success of later measurements. An ideal specimen should be: (i) a representative, thin area of a typical bulk sample; (ii) largely flat, undamaged by preparation; (iii) easy to handle and not too fragile; (iv) stable, clean and conducting. [105]

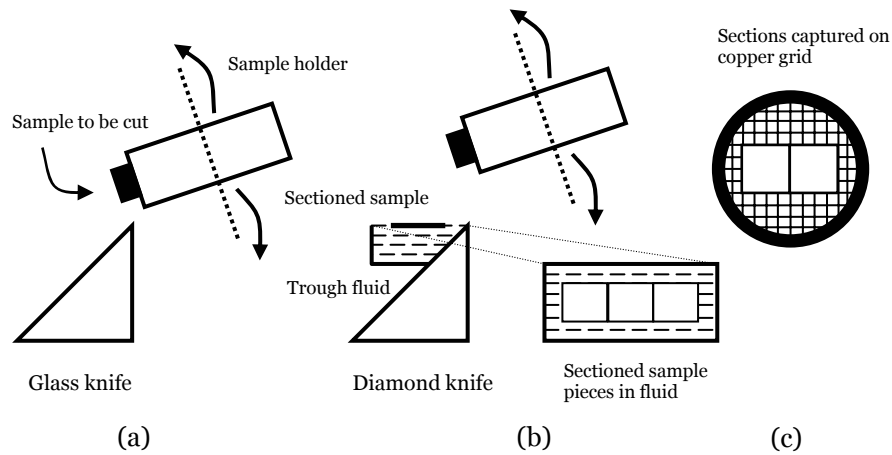


Figure 8.4: Schematic plot of TEM sample preparation steps: (a) 1<sup>st</sup> step: sample trimmed by glass knife; (b) 2<sup>nd</sup> step: sample further trimmed by diamond knife and floated in fluid and (c) sections captured on copper grid.

The 1.5 GPa treated samples studied in this work (sPI and MWCNT/sPI composite) are fairly hard and therefore possible to cut directly without further treatment. Thin sections for TEM studies were obtained by ultramicrotome sectioning. [105] The procedure included gluing the specimen on epoxy resin, trimming, 1<sup>st</sup> sectioning by glass knife (Figure 8.4a) and 2<sup>nd</sup> sectioning by diamond knife (Figure 8.4b). The thickness of sections can be roughly estimated by the interference colors when the sections are floating on the liquid (Figure 8.4b), e.g. a color change from silver to grey indicates a thickness change from 70 to 40 nm. [104] The most suitable sections are later captured and transferred to a copper grid and air dried (ca. 24 h). The grids (coated with a 35 nm thick carbon film, 300 mesh, Pacific Grid Tech) are 3.05 mm diameter circles made of copper, containing a square array of bars (hole size: ~63  $\mu\text{m}$ , Figure 8.4c). Since CNTs are easily distinguished from the polymer in TEM images, it is easy to assess the degree of dispersion of the CNTs in the matrix without further etching or staining steps.

It is easy to prepare neat CNT samples since CNTs can be dispersed in a solvent and dripped on a TEM grid with a support coating film. A typical preparation procedure includes: dispersing CNT in ethanol (or toluene) using bath sonication (or ultrasonic pin) for 5 minutes, dropping a small

amount of the mixture on a copper grid (with carbon film coating) and drying for 24 h prior to measurements.

### **8.3 Scanning electron microscope**

A SEM is a type of electron microscope that images a sample by scanning it with a high-energy beam of electrons, similar as TEM (Figure 8.3b). The electrons interact with the atoms at the sample surface mainly by scattering and the scattered electrons provide information about the surface topology. As the electrons do not pass through the sample, no sectioning is needed. The secondary electrons (normal imaging mode, detect ca. 10 nm in depth) and backscattered electrons (commonly used together with X-ray spectra for element analysis) are used for sample imaging. Therefore only surface information is collected during imaging. On the other hand, due to a large depth of field, SEM images have a characteristic three-dimensional appearance. Moreover, SEM can be used for fractography analysis, in which the fractured surface requires only a conductive coating layer; orientation studies of fiber sample and phase morphology of polymer/polymer blended samples.

#### ***8.3.1 Sample preparation: coating with gold***

Due to the low conductivity of polymers, a thin layer of an electrically conducting material, e.g. gold or silver, is coated on the sample prior to measurement. In this work, the coating was achieved by vacuum evaporation of gold. The specimen was glued to a metal plate and mounted on a metallic sample holder, which was used as grounded electrode. The coating layer was about 20 nm in thickness. It is worth pointing out that the coating can enlarge the size of features observed by SEM.

### **8.4 Optical microscope**

An OM is a microscope that magnifies small objects by lenses using a visible light source, and it has a resolution of typically a few micrometers. An OM was used to get a preliminary assessment of the CNT dispersion in the composite samples, which were prepared using a high power ultrasonic processor. The samples were spin coated or drop cast on glass slides for the OM studies. This was the first step to examine the dispersibility of the CNTs in the polymers and to find the most suitable parameters to disperse the CNTs. 'Optically dispersed' is defined as no agglomeration or phase separation was observed by OM when CNT is dispersed in a polymer matrix.

## 8.5 Nuclear magnetic resonance

Nuclear magnetic resonance (NMR) spectroscopy is a powerful tool providing structural and dynamical information of material at atomic level, making it an ideal tool in material science, physics, medicine and biological researches. [106]

The most common nuclei used in NMR for materials science are the  $^1\text{H}$  and  $^{13}\text{C}$  nuclei. In general, the NMR can detect these nuclei which possess a spin of  $1/2$  and possess therefore a permanent nuclear magnetic moment. In the case that the sample is placed into a permanent magnetic field ( $B_0$ ), the nuclear magnetic moments of these nuclei are going to adopt different positions with respect to  $B_0$ . A nucleus with a spin of  $1/2$  adopts two possible alignments (Figure 8.5) corresponding to the two allowed magnetic quantum states, with  $m=1/2$  being the lower energy state whereas  $m=-1/2$  being the higher energy state (Figure 8.5). By sending a radio frequency pulse at a certain frequency that corresponds to the energy difference  $\Delta E$ , it is possible to flip the nuclear spins from  $E_1$  to  $E_2$  state.

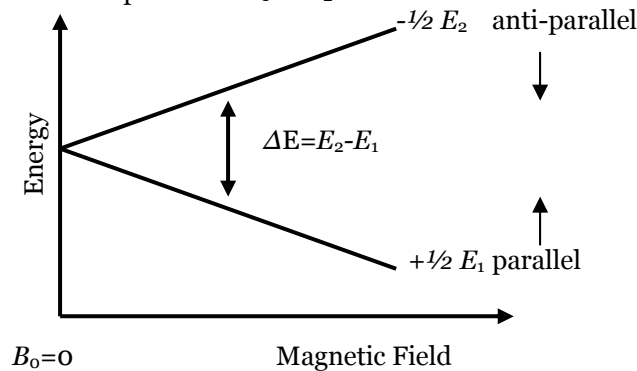


Figure 8.5: Energy level for a  $1/2$  spin. [107]

Before applying NMR radio frequency pulse sequence, the sample has a macroscopic initial magnetization,  $M_z$  due to a population difference between the magnetic nuclear spins which are aligned parallel to the  $z$  axis ( $B_0$  axis) and the ones being aligned antiparallel (Figure 8.6). In a typical NMR experiment, the perturbation of this macroscopic magnetization vector is conducted by applying a  $90^\circ$  radio frequency pulse along the  $x$  axis. The  $M_z$  aligned along the direction of  $B_0$  is flipped from  $z$  axis to  $x$ - $y$  plane, as shown in Figure 8.6. The oscillating of magnetization can be recorded as an alternating voltage in the detection coil. This NMR signal is called free induction decay (FID).

The collected FID is the time-dependent decay of the transverse magnetization,  $M_{XY}$  and can be converted into the frequency domain – the NMR spectrum – by Fourier transformation. [108] In general, this magnetization which processes at the Larmor frequency of the specific nucleus to be observed, diminish in  $x$ - $y$  plane due to the loss of spin coherence, a phenomenon described as spin-spin relaxation and characterized by the spin-spin relaxation time  $T_2$  according to:

$$M_{XY} = M_{XY0} e^{-t/T_2} \quad (8.1)$$

where  $M_{XY0}$  is the transverse magnetization at time zero.

In addition, there is a process of the return of the longitudinal magnetization  $M_Z$  towards its equilibrium (as before an NMR pulse). This process is called spin lattice relaxation with a characteristic time,  $T_1$ , and described as:

$$M_Z = M_0 (1 - e^{-t/T_1}) \quad (8.2)$$

where  $M_0$  is the longitudinal magnetization at the thermal equilibrium.

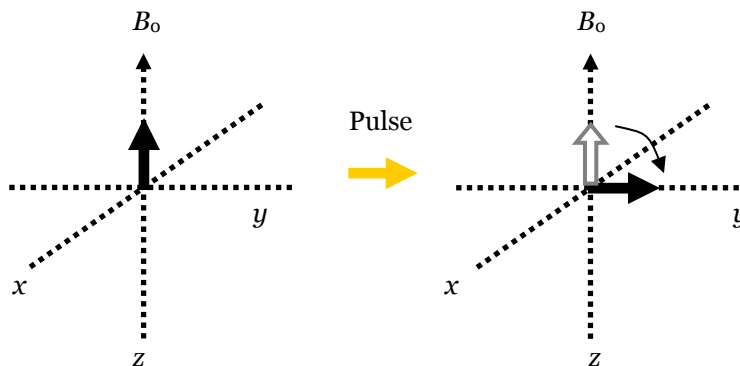


Figure 8.6: NMR coordinate system. [107]

### 8.5.1 Chemical shift

In general, nuclei of the same species (e.g. protons) can have a different electronic environment due to variations in their chemical molecular surroundings. These differences yield a variation in the reduction of the outer field at the location of a specific nucleus, causing differences in the observed Larmor frequency. This so-called chemical shift is indicative of the

immediate chemical environment of the nucleus and therefore ideal to localize the nucleus as part of the specific molecular segment e.g. therefore the information of microstructure of material can be extracted by converting the chemical shift variations into different chemical environments for a nucleus in a sample. Since  $B_0$  differs between spectrometers, the frequency measurement in Hz is converted to a standard chemical shift scale that measures in parts per million (ppm). In this way the chemical shift in NMR can be universally compared in ppm. The chemical shift is calibrated using an internal standard, such as tetramethylsilane (TMS). But frequently an external reference of known chemical shift can be used instead of TMS. In this thesis adamantane is used as  $^{13}\text{C}$  standard for solid state NMR studies. The chemical shift is obtained by using:

$$\delta = (\nu - \nu_0) / \nu_0 \quad (8.3)$$

where  $\delta$  is the chemical shift,  $\nu$  is the resonant frequency and  $\nu_0$  is the standard frequency.

### **8.5.2 Magic angle spinning**

The line width of an NMR resonance depends on orientation factors, i.e. chemical shift, chemical shielding anisotropy, magnetic susceptibility and susceptibility differences within sample. For a solid sample, due to low molecular mobility (comparing to high molecular mobility and re-orientation movement of liquid state NMR), the typical solid state NMR spectrum is the result of an overlap of many NMR signals from molecules at different orientations with respect to the magnetic field, causing broad featureless spectra without significant resolution. Due to the anisotropic feature of solid sample where most line-broadening interactions can be described by a second rank tensor, Magic Angle Spinning (MAS) around  $54.74^\circ$  is often applied to average the 2<sup>nd</sup> Legendre Polynom  $P_2(\cos\theta)$  to zero, with  $P_2(\cos\theta) = (3\cos^2\theta - 1)/2$ . Therefore most anisotropic interactions disappear and the NMR spectrum will break up in a series of individual isotropic narrow lines as in liquid NMR, thereby allow assignment of the individual resonances to specific chemical groups as in liquid NMR.

### **8.5.3 Cross-polarization**

Cross-polarization (CP) is a technique typically used in solid-state NMR to enhance the signal of dilute spins. [109] CP is often combined with MAS methods to achieve a better resolution and sensitivity in solid-state NMR spectra, in order to overcome the problem of low natural abundance of  $^{13}\text{C}$  as well as low sensitivity of  $^{13}\text{C}$  in total in the HP&HT treated sample. Moreover, CP can be used to identify whether the  $\text{C}_{60}$  is covalently bonded to PI after

treatment. [110] The CP pulse sequence is conducted by first applying a  $90^\circ$  pulse to a high abundance spin, normally  $^1\text{H}$ , followed by a  $^1\text{H}$  spin-lock pulse to maintain the magnetization and simultaneously the application of a contact pulse on the low abundance nuclei ( $X$ ), for example  $^{13}\text{C}$  as shown in Figure 8.7. This procedure causes a transfer in magnetization when the nutation frequencies of both the  $^1\text{H}$  and  $^{13}\text{C}$  magnetization vectors are matched (Figure 8.7). The gaining of signal is ca. 4 times better than without CP pulse.

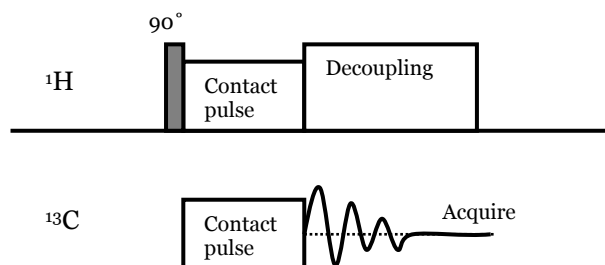


Figure 8.7: A typical CP pulse sequence.

#### 8.5.4 Measurement of spin-spin relaxation time

The measurement of  $T_2$  values in solids can be carried out by Hahn-echo pulse sequences with a typical  $90^\circ$ - $\tau$ - $180^\circ$ - $\tau$ -acquire- sequence delay. The signal relaxes further with increasing  $\tau$  value before signal acquisition. By fitting the signal intensity to an exponential function  $\exp(-2\tau/T_2)$ ,  $T_2$  is obtained. [111] In this thesis, the  $T_2$  is used to characterize the cross-link level of PI at different treatment pressure. [93] For a non-cross-linked or low cross-linked polymer, the relaxation process is rather long (the molecular chain is more flexible) therefore the  $T_2$  is long. However, in a highly cross-linked polymer (the cross-links restricted the movement of polymer chain), e.g. 1.5 GPa treated PI, the spin-spin relaxation process becomes more dominant, therefore short  $T_2$  was obtained. Moreover, the  $T_2$  measured for different PI is qualitatively in agreement with swelling results.

## 8.6 Wide angle X-ray diffraction

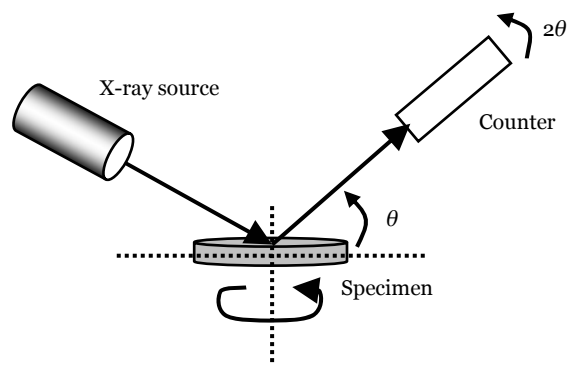


Figure 8.8: Schematic plot of WAXD setup.

Wide angle X-ray diffraction (WAXD) is applied to examine the crystal structure of samples at relatively large scattering angles. As shown in Figure 8.8, the stage rotates  $\theta$  meanwhile as the signal receive arm rotates  $2\theta$ . In addition, the stage can rotate in the panel as indicated to ensure a homogenous sample scanning. In this thesis, WAXD was carried out using a Siemens/Bruker D5000 diffractometer with  $\text{CuK}\alpha$  radiation at an acceleration voltage of 40 KV and a tube current of 30 mA. The samples were scanned twice from  $5^\circ$  to  $50^\circ$  ( $2\theta$ ) at scanning rate of  $4^\circ$  per minute. As observed in Paper I, [52] II [112] and III, [113] the crystals of a semicrystalline polymer (nylon 6) can attain a preferred orientation after HP&HT treatment. Therefore two scans were performed for two different purposes. The first scan was done on the recovered sample after the HP&HT treatment (Figure 8.8), and the second after the sample had been manually chopped into small grains. The first WAXD spectra were used to determine the preferred pressure induced crystal orientation and the second were used to determine the degree of crystallinity (mass fraction),  $C_{\text{WAXD}}$ , and crystallite size and perfection (*CSP*).  $C_{\text{WAXD}}$  was obtained from: [51]

$$C_{\text{WAXD}} = A_c / (A_c + A_a) \quad (8.4)$$

where  $A_c$ ,  $A_a$  are the integral area of the crystalline and amorphous peak intensities, respectively, which were obtained through fits by Peakfit® software.

*CSP* were determined by the Scherrer equation: [51]

$$CSP = k\lambda / (\beta \cdot \cos \beta) \quad (8.5)$$

where  $\beta$  is the width of the crystalline peak at  $2\theta$ ;  $\lambda$  is the X-ray wavelength (0.154 nm);  $k$  equals to 0.9 when  $\beta$  is the full width at half maximum.

## 8.7 Vibrational spectroscopy

Vibrational spectroscopy was applied to characterize the vibrations of the molecules, such as changes in bond length, bond angle or torsion angle etc. The Raman shift is in many cases consistent with the absorption in Fourier transform infrared spectroscopy (FTIR) spectra but some vibrations may not be both Raman and FTIR active and thus appear only in one of the spectra. In general, FTIR is more sensitive to highly polar groups whereas Raman scattering is more sensitive to non-polar groups. Both Raman spectroscopy and FTIR can also provide information on the crystallinity of a sample, [51] but the information is more or less only qualitative.

### 8.7.1 Raman spectroscopy

When laser light interacts with molecular vibrations, phonons or other excitations in the system, the energy of the laser photons is shifted up or down. The shift in energy provides information about the vibrational modes in the sample, as shown in Figure 8.9. Raman spectroscopy is a technique to study inelastic scattering of laser light in a sample, and if phonon loses or gains energy in a scattering process, it is referred to as Stokes and anti-Stokes Raman scattering, respectively, as shown in Figure 8.9. Spontaneous Raman scattering is typically very weak compared to Rayleigh scattering and, as a result, the main difficulty of Raman spectroscopy is separating the weak inelastically scattered light from the intense elastically scattered Rayleigh light.

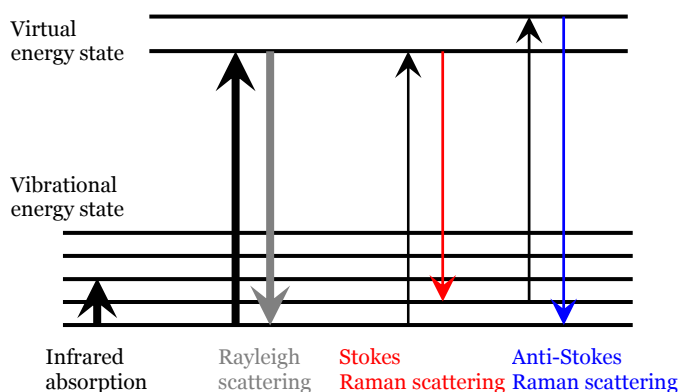


Figure 8.9: Energy level diagram showing the states involved in Raman and infrared signals. The thickness of lines in the figure is roughly proportional to the signal intensity from different transitions.

The Raman shift is calculated based on the expression:

$$\Delta\omega = \left( \frac{1}{\lambda_0} - \frac{1}{\lambda_1} \right) \quad (8.6)$$

where  $\Delta\omega$  is the Raman shift expressed in wavenumber,  $\lambda_0$  is the excitation wavelength, and  $\lambda_1$  is the Raman spectrum wavelength. The unit of Raman spectra is inverse centimeters ( $\text{cm}^{-1}$ ).

The Raman setup mainly used in this thesis (Renishaw 1000 grating spectrometer) is shown in Figure 8.10. Light from the illuminated spot is collected with a lens and sent through a monochromator to an optical microscope. The microscope is equipped with short (20, 50X) and long distance view (5, 20 and 50X) lenses for different measurement occasions. [46] The position of the laser spot is controlled by a microscope stage and monitored by a video camera. The back-scattered light, i.e. after interfering with a specimen, is detected by a CCD detector. The wavelengths close to the laser line due to elastic Rayleigh scattering, are filtered out by a Notch filter while the rest of the collected light is dispersed onto the detector.

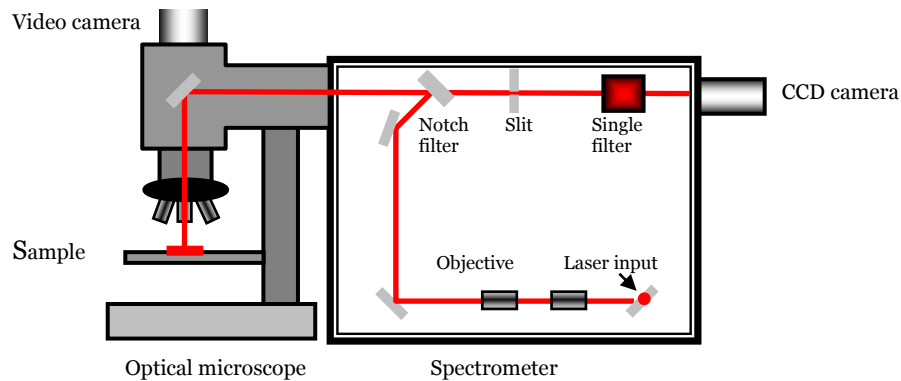


Figure 8.10: The optical route and setup of Raman measurement system. [114]

The Raman setup in Dept. of Physics includes three lasers, Infrared (invisible, 830 nm), He-Ne (red, 632 nm) and Argon-ion lasers (green, 514 nm). Using He-Ne or Argon-ion laser, the spectrometer can collect the spectra in the range from 3500 to 100  $\text{cm}^{-1}$  whereas the Infrared laser can collect from ca. 1800 to 100  $\text{cm}^{-1}$ . Recently, a new Raman spectrometer

(Renishaw inVia) was established with a more sophisticated and improved hardware and software.

It is well established that CNTs show a Raman peak at ca.  $1600\text{ cm}^{-1}$  due to the tangential vibrational mode which is characteristic of graphite (G mode), and a Raman peak at ca.  $1300\text{ cm}^{-1}$  due to defects (D mode). [115, 116] This information of MWCNTs/SWCNTs was used in early state of this thesis work in the analysis of the purity of the CNTs before and after purification processes. Later, Raman spectroscopy was applied to study cross-linking and chain scissoring of nylon-6 samples. [52] Besides, Raman spectroscopy was used to study the interaction between CNT fillers and polymer matrixes. CNTs have a Raman active vibration in the range of  $2500\text{-}2700\text{ cm}^{-1}$  (denoted as  $D^*$ -vibration), which is sensitive to strain or stress. [117, 118] This was used to study the interaction between MWCNTs and highly cross-linked LPB, and a significant shift of the  $D^*$  vibration was detected after cross-linking. [119]

### ***8.7.2 Fourier transform infrared spectroscopy***

The principle of FTIR is to measure the absorbed light of a sample as a function of wavelength. The absorption frequencies correspond to certain vibrational modes of the sample molecules and a FTIR spectrum therefore provides a unique signature of the sample. Measurements in this thesis were performed in attenuated total reflection (ATR) mode. The ATR mode needs almost no sample preparation in contrast to transmission mode, which requires thin film samples ( $\sim 100\text{ }\mu\text{m}$ ). Irregularly shaped solid bulk samples can be easily clamped in the ATR setup, as shown schematically in Figure 8.11, whereas liquid samples or solvents are kept in a Teflon<sup>®</sup> cell for quick measurement. As shown, the incident beam reflects many times against the sample before detection, which enhances the sensitivity. In order to limit disturbances of carbon dioxide in the air, a protective nitrogen atmospheric environment (nitrogen flow) is created for measurement and a reference scan (empty scan, without sample) is performed before sample measurement. A typical FTIR measurement was performed in 'transmittance mode' (or inversely called 'absorption mode') to characterize how much of the incident beam was transmitted (or inversely absorbed) by the sample in the range of  $4400\text{-}600\text{ cm}^{-1}$  with a resolution of  $1\text{ cm}^{-1}$ .

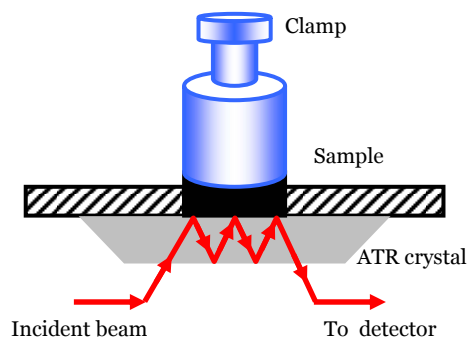


Figure 8.11: Sample arrangement for ATR mode in FTIR.

### 8.8 Differential scanning calorimetry

Differential scanning calorimetry (DSC) is a thermoanalytical technique used to characterize the difference in the amount of heat as a function of temperature required to increase the temperature of a sample and a reference. The temperature of the sample container is kept the same as that of the reference container by a continuous and adjustable heat power. The power difference between the sample and reference is recorded. The containers are heated individually and the temperatures are measured by Pt sensors as indicated in Figure 8.12.

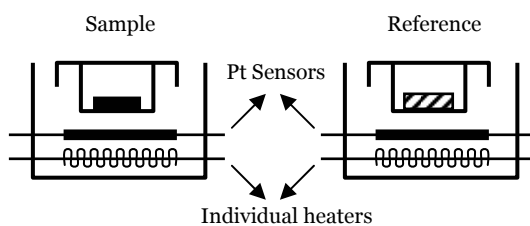


Figure 8.12: Schematic plot of a typical DSC setup.

DSC was applied to evaluate changes in crystallinity and transition behavior of the high pressure treated composites and polymers. The samples were scanned at heating and cooling rates of typically 10 °C per min. From the measured DSC signal,  $T_g$ ,  $T_{melt}$ , melting onset temperature ( $T_{onset}$ ), melting enthalpy ( $\Delta H$ ) and  $T_{cry}$  etc. could be obtained, as shown in Figure 8.13.

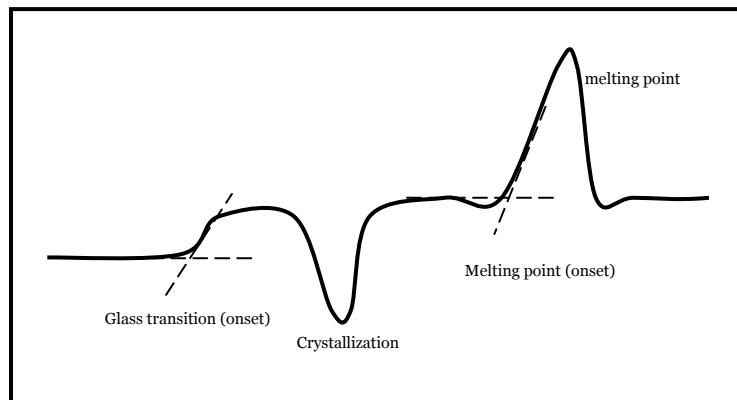


Figure 8.13: A schematic plot of a typical DSC curve showing several types of transitions: glass transition, melting and crystallization.

The degree of crystallinity  $C_{DSC}$  (mass fraction) was calculated from heat of fusion using the total enthalpy ( $\Delta H$ ) method, which yields: [49]

$$C_{DSC} = \Delta H / H_{100\%} \cdot 100\% \quad (8.7)$$

where  $\Delta H$  is the melting enthalpy ( $J\ g^{-1}$ ) of polymer (in the case of a composite, the weight of filler needs to be accounted for) and  $H_{100\%}$  is the extrapolated value for the melting enthalpy of 100% crystalline polymer, which was here obtained from literature data.

A Pyris Diamond DSC equipped with intra-cooler was used for DSC measurements. The samples were encapsulated in aluminum pans. For the water and oxygen sensitive polymer nylon-6, the sample was pumped 24 h in a vacuum oven and encapsulated under a dry nitrogen/argon atmosphere at room temperature to limit the water and oxygen. In this work, the nylon-6 samples were heated from 20 to 250 °C (ca. 20 °C higher than  $T_{melt}$  of nylon-6) at a scan rate of 10 °C per minute and held at 250 °C for 5 minutes to ensure that the samples were melted before cooling. Subsequently, the samples were cooled to 20 °C using the same scan rate.

## 8.9 Cross-link density measurement

The cross-link density is an important factor for the properties of network polymers such as PI and PB. Various methods were adopted to measure the cross-link density of the samples in order to overcome the limitation of each method. For example, the swelling method detects both chemical and physical cross-links, whereas NMR can be used to evaluate the number of chemical cross-links.

### 8.9.1 Cross-link density via swelling

Cross-link density of PI, SWCNT/sPI, MWCNT/PI and C<sub>60</sub>/PI samples were determined using the swelling method ( $v_{\text{swell}}$ ) which determines the average molecular weight between cross-links ( $M_c$ ). The relation between  $M_c$  and  $v_{\text{swell}}$  is expressed as: [120]

$$v_{\text{swell}} = \rho / (2 \cdot M_c) \quad (8.8)$$

where  $\rho$  is the density of sample.

In a typical swelling measurement, the samples were soaked in either *n*-heptane or toluene at room temperature for 48 h, which should be long enough for the sample to reach equilibrium. [121] The cross-link density is estimated by the Flory-Rehner equation:[122, 123]

$$v_{\text{swell}} = -[\ln(1 - \phi) + \phi + \chi\phi^2] / [2V_s (\phi^{1/3} - 2\phi / f)] \quad (8.9)$$

where  $v_{\text{swell}}$  is the crosslink density (mol cm<sup>-3</sup>),  $\phi$  is the volume fraction of the network polymer in the swollen sample,  $V_s$  is the molar volume of the solvent,  $f$  is the functionality of the cross-linked network, here assumed to be a perfect tetrafunctional network, i.e.  $f=4$ , and  $\chi$  is the polymer-solvent interaction parameter. [124, 125] The volume fraction is calculated from:

$$\phi = [(m_d - m_f) / \rho] / \{ [(m_d - m_f) / \rho] + [(m_s - m_d) / \rho_s] \} \quad (8.10)$$

where  $m_d$ ,  $m_f$  and  $m_s$  are the masses of the sample dried after swelling, filler in the sample and the swollen sample respectively,  $\rho$  is the density of the polymer, and  $\rho_s$  is the density of the solvent.

In Paper VI, evidence is found for a polymer layer wrapped/coated on the CNTs, which proposes that this layer limits the swelling. To test the assumption, eq. 8.10 was modified to account for a non-swelling layer by calculation of  $\phi$  from: [93]

$$\phi = [(m_d - m_f - m_i) / \rho] / \{ [(m_d - m_f - m_i) / \rho] + [(m_s - m_d) / \rho_s] \} \quad (8.11)$$

where  $m_d$ ,  $m_f$ ,  $m_s$  and  $m_i$  are, respectively, the masses of the sample dried after swelling, the filler, the swollen sample and the inter-phase layer.

### 8.9.2 Cross-link density via Young's modulus

The cross-link density can also be estimated from  $E$  ( $\nu_E$ ). Gent and Kaang [126] proposed an equation to calculate  $M_c$ :

$$M_c = 3\rho RT / E \quad (8.12)$$

where  $R$  and  $T$  are the gas constant and temperature respectively;  $\rho$  is the polymer density measured by Archimedes' principle.  $E$  is extracted from tensile testing (see Chapter. 7). The  $\nu_E$  is calculated from  $M_c$  as eq. 8.8.

### 8.9.3 Cross-link density via NMR

NMR results were used to calculate the cross-link density ( $\nu_{NMR}$ ) of sPI and MWCNT/sPI composite by assuming that one broken double bond (C=C) during the HP&HT treatments resulted in one cross-link. The consumption of double bonds was estimated from the area of the NMR signal before and after the HP&HT treatment. With these assumptions, the following was found: [93]

$$\nu_{NMR} = \frac{D_{before} - D_{after}}{D_{before}} \cdot \frac{\rho}{M_{Polymer}} \quad (8.13)$$

where  $D_{before}$  and  $D_{after}$  are the ratios of the double bonds peak area against total peak area in the NMR spectra before and after HP&HT treatment, respectively;  $M_{Polymer}$  is the molecular weight of one repeat unit of polymer containing one double bond, and  $\rho$  is polymer density.

### 8.9.4 Cross-link density via gel formation

HP&HT treated nylon-6 were immersed in formic acid (puriss, 98.0-100%, Sigma-Aldrich) to study gel formation, which takes place if the sample is cross-linked. Weighed nylon-6 samples were immersed in 85% formic acid solution for 3 days at room temperature, as suggested by Sengupta et al. [127]. The gel content can be calculated from: [127]

Gel content (%) = Un-extractable fraction / Total sample weight (8.14)  
after being collected by filtering through a fritted glass crucible. However, in Paper I, II and III, all the nylon-6 or nylon-6 based CNT/nylon-6 composites were dissolved in 85% formic acid solution, which suggested that there were no cross-links in the samples.

## 8.10 Viscosity measurement

Viscosity measurement was done via a falling-ball viscometer (Thermo Scientific HAAKE Falling Ball Viscometer type B) at 25.0 °C. The temperature was maintained with water bath (Grant Instruments Ltd).

To determine the viscosity-average  $M_w$  of nylon-6, nylon-6/85% formic acid (puriss, 98.0-100%, Sigma-Aldrich) solutions were prepared with the solute (nylon-6) concentrations up to 0.5 g/100 ml. Viscosity-average  $M_w$  was calculated from the Mark-Houwink equation: [128]

$$[\eta] = KM_w^a \quad (8.15)$$

where  $[\eta]$  is the intrinsic viscosity,  $a$  and  $K$  are constants that depend on the particular polymer-solvent system and the temperature. [129] In 85% formic acid at 25 °C,  $a=0.82$  and  $K=2.26 \times 10^{-4} \text{ dl g}^{-1}$ . [129] The intrinsic viscosity is equal to the reduced viscosity,  $\eta_{\text{reduced}}$ , extrapolated to zero solute concentration, and  $\eta_{\text{reduced}} = (\eta - \eta_0)/(c \cdot \eta_0)$ , where  $\eta$  is the dynamic viscosity of the solution,  $\eta_0$  is the dynamic viscosity of the solvent, and  $c$  is the solute concentration ( $\text{g dl}^{-1}$ ). [51]

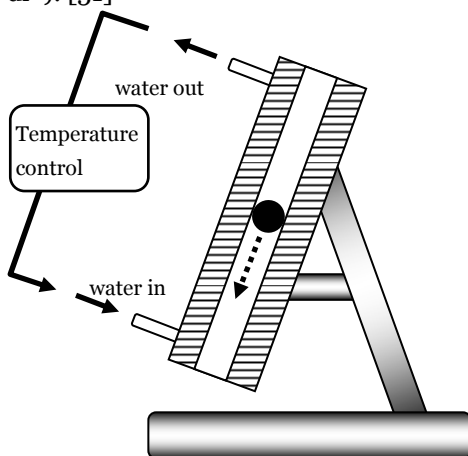


Figure 8.14: Schematic plot of viscometer setup.

The dynamic viscosity ( $\eta$ , in cP) of the solution and the solvent were obtained from falling-ball viscosity measurements. Approximately 40 cm<sup>3</sup> solution was poured into a slightly tilted-arranged measuring tube, as shown in Figure 8. 14. In one measurement, the time was recorded when the ball was falling from the top to the bottom mark of the tube. To ensure accuracy, each sample was measured 5 times and the average of time was used. The equation for  $\eta$  is given by: [130]

$$\eta = t \cdot (\rho_1 - \rho_2) \cdot K \quad (8.16)$$

where  $t$  is the measured falling time of the ball in seconds,  $K$  is the ball constant (ball No.2, 0.05212 mPa·s·cm<sup>3</sup>/g·s) as supplied by the manufacturer;  $\rho_1$  (2.216 g/cm<sup>3</sup>) and  $\rho_2$  are the densities of the ball and the solution, respectively. The density of the solution was measured by

transferring and measuring the weight of 20 ml of solution by a 20 ml volumetric pipette.

### 8.11 Density measurement

Mass density of solid samples was measured by the Archimedes' principle by quickly immersing samples in water as well as by submerging in various methanol/water mixtures kept at 25 °C, with an estimated inaccuracy of  $\pm 0.5\%$ . In the latter case, the density of the sample is equal to that of the mixture when the sample is suspended in the solution.

The degree of crystallinity (mass fraction) extracted from density of semicrystalline polymer,  $C_p$ , was determined from the equation: [131]

$$C_p = \left( \frac{1}{\rho_\alpha} - \frac{1}{\rho} \right) / \left( \frac{1}{\rho_\alpha} - \frac{1}{\rho_c} \right) \cdot 100\% \quad (8.17)$$

where  $\rho$  is the measured density of the polymer by immersing in water,  $\rho_\alpha$  and  $\rho_c$  are the density of the amorphous and crystalline phase of the polymer respectively. In the case of a composite, the density of filler needs to be accounted for by:

$$\rho_{composite} = \frac{1}{\frac{w_{Polymer}}{\rho_{Polymer}} + \frac{w_{Filler}}{\rho_{Filler}}} \quad (8.18)$$

where  $w$  is the weight fraction and  $\rho$  is the density of polymer and filler, respectively.

### III. Summary of the included papers

In this section, I summarize the papers included in this thesis and describe my contributions to each publication.

The papers included in this thesis are based on the idea to use HP&HT treatment to modify two of the most important characteristics of polymers: cross-link density and crystallinity, as well as to study the effect of strong densification. First the properties of the pure polymers were established: e.g. nylon-6 (Paper I) and PB (Paper VII), and thereafter those of their nanocomposites: MWCNT/nylon-6 composites (Paper II and III), CNT/PI composites (Paper IV, V and VI), CNT/PB composites (Paper VIII) and C<sub>60</sub>/PI composites (Paper IX).

#### Paper I, II and III

HP&HT treatment can drastically increase the crystallinity of semi-crystalline polymers. Nylon-6 was studied in Paper I to investigate both possible cross-linking and increased crystallinity by HP&HT treatments. There was no indication of cross-linking but instead a strongly increased crystallinity. The effect of crystallinity and CNT fillers was thereafter studied in a MWCNT/nylon-6 in Paper II and III. For pure nylon-6, the crystallinity of the polymer could be increased from ~35% to 55-60% after a cold crystallization process caused by HP&HT treatment. Concurrently, the microstructure of nylon-6 was modified such that the crystals attained a preferred orientation and scissoring decreased the average chain length.

For P-MWCNT filled nylon-6 (P-composite), the cold crystallization increased the crystallinity from 31 to 58% after 1.0 GPa treatment. A more sluggish time evolution of the process than that for pure nylon-6 indicated that MWCNTs slightly disrupted the crystallization process. As a result of the increased crystallinity,  $\kappa$  of the P-composite increased ~37%. Moreover, the HP&HT treatment produced a more thermally stable state, in which the P-composite obtained a distinctly higher  $T_{\text{melt}}$  than nylon-6 treated at identical conditions. The improved stability was attributed to large nylon-6 crystals with reinforcing CNT bridges in between.

In addition, the nylon-6 and its composite were studied by reversible densification by *in-situ* hot-wire measurements. The pressure-dependence of  $T_g$  of nylon-6 and P-composite was established despite that  $T_g$  of nylon-6 is unusually difficult to detect.

The results showed that MWCNT slightly promote  $T_g$ . Furthermore, the MWCNT promoted  $\kappa$  of the P-composite by 13%/wt% MWCNT. It was also deduced that the interfacial thermal resistance at the CNT-polymer interface decreased with increasing pressure. Despite the decrease, the interfacial

thermal resistance is still large and responsible for the relatively low increase of  $\kappa$  after adding MWCNTs.

In paper I, II and III, I performed most of the experimental works, including syntheses and characterization (*in-situ* hot-wire measurements, DSC, WAXD, AFM, and TEM analyses) of nylon-6 and MWCNT/nylon-6 composite. In paper II and III, I and Gerhard Gröbner performed NMR analyses of MWCNT/nylon-6 composite. All authors were involved in the evaluation of the results. I wrote the first version of the manuscripts together with Ove Andersson.

## **Paper IV, V and VI**

Besides the capability of crystallizing polymers, HP&HT treatment can modify the cross-link density of a polymer. PI was selected as a matrix based on a previous publication of a similar polymer (PB) had shown that HP&HT treatment could be used to cross-link a polymer without the use of chemicals. [132] A study on pure sPI confirmed that sPI could also be cross-linked. [56]

Results of SWCNT/sPI composites, presented in Paper IV, showed that HP&HT treatment changed the molecular mobility significantly. For example, the SWCNT filler (5 wt %) increased  $T_g$  of the elastomeric (cross-linked) state by as much as 12 K. The swelling method suggested a significantly higher cross-link density in the composite than in neat sPI after identical HP&HT treatment. At this time, we thought that the SWCNTs may have increased the chemical cross-link density, and that this was the main reason for the much higher  $T_g$  of the composite. However, our later studies suggest that this increase was due to physical cross-links/constraints caused by the CNT-polymer interaction.

The study also concerned the  $\kappa$ , and showed that 5 wt% SWCNT promoted  $\kappa$  by 120 % (24%/wt%CNT), which is the largest increase for all the matrices studied here (PB and nylon-6). Last but not the least, a distinct decrease of the heat capacity (~30%) was observed in both the untreated and the elastomeric state of the composite.

Paper V and VI mainly concerned the promoted tensile properties of SWCNT (MWCNT)/PI composites by HP&HT treatment. The increased tensile properties of SWCNT/sPI composite were first observed in the study of Paper V. A composite with 5 wt% SWCNTs showed 2.2 higher tensile strength  $\sigma_{UTS}$  ( $\sigma_{UTS}=17$  MPa), 2.3 times higher Young's modulus  $E$  ( $E=220$  MPa) and longer extension at break than pure sPI. The improvement occurred concurrently with increased cross-link density, as measured by the swelling method. But in this work, there were noticed features that suggested that the (chemical) cross-link density of the composite was lower than that of the neat polymer. The cross-link density levelled off at high SWCNT dosages

and the composites showed longer extension at break up to about 5wt% CNTs. The former suggested that the high cross-link densities were associated with the surface area of the CNTs. Moreover, the increased extension suggested that the chemical cross-link density was actually lower in the composites, and we conjectured that the CNTs disrupted chemical cross-links, which reduced the brittleness and gave an effect similar to crazing, i.e. bridging of micro-cracks by polymer fibrils. This conjecture was also supported by SEM images.

In Paper VI, the high cross-link densities of the composites and an observed correlation between cross-link density (from swelling measurements) and the reinforcement of CNTs was further illuminated and described by a model. NMR measurements were employed and showed evidence that the chemical cross-link density in the composites was more or less the same or even lower than that in pure sPI treated at identical conditions. The increased cross-link density was instead attributed to physical CNT-polymer interactions, or so-called physical cross-links/constraints that limit swelling. The results of Paper VI suggested that these physical cross-links were reflected in the extent of polymer coating and that these also assisted the reinforcement of the composites. The model links the thickness of a strongly bound interfacial polymer layer to the mechanical properties of the composites with a correlation which is almost independent of the types of CNTs and CNT content. The layer seemed augmented by treatment under high pressure, as indicated by swelling measurements and AFM images.

The strongest composites were produced by treatment at 1.5 GPa, e.g. the  $\sigma_{UTS}$  and  $E$  of sPI increased 2 times by adding 3 wt% MWCNTs. The study suggested that high pressure can be used to promote polymer wrapping/coating of CNTs and that the phenomenon is important for the mechanical properties of CNT/polymer composites.

In Paper IV, I performed TEM analyses of SWCNTs and contributed to the evaluation and discussion of the results. In Paper V, I carried out AFM and SEM analyses (together with Britt Andersson) of SWCNT/sPI composites and took part in the evaluation and discussion of the results. In Paper VI, I synthesized MWCNT/PI composites, conducted HP&HT treatment of composites at 1.5 GPa, performed the tensile tests, AFM&TEM imaging and swelling experiments. I and Gerhard Gröbner performed NMR analyses of sPI and MWCNT/sPI composites. Bounphanh Tonpheng performed the studies of sPI and MWCNT/sPI composites from 0.25 to 1.2 GPa (synthesis, HP&HT treatment, tensile tests and swelling experiments). All authors were involved in the evaluation of the results. I wrote the first version of the manuscript together with Ove Andersson.

## Paper VII and VIII

As mentioned above (in Paper IV), the elevated cross-link density caused by HP&HT treatment raised the  $T_g$  significantly and improved the mechanical properties of sPI and SWCNT/sPI composites. However,  $\kappa$  and  $\rho c_p$  did not change during the cross-linking process. To monitor the process and investigate the effect of higher cross-link densities, PB was chosen to study since it is more reactive than PI.

In Paper VII,  $\kappa$ ,  $\rho c_p$  and the glass transition behaviour under pressure were established for medium (sPB) and high vinyl content (LPB). Their highly cross-linked (ebonite like) states were also investigated after cross-linking purely by HP&HT treatments. The results showed that cross-linking eliminated the glass transitions and increases  $\kappa$  by as much as 50% at 295 K and 1 atm. The pressure and temperature dependencies of  $\kappa$  were also strongly changed by cross-linking, which increased the effect of temperature but decreases the effect of pressure. We attributed these changes to a cross-linked induced permanent densification and a consequential increase of phonon velocity simultaneously as conduction along polymer chains was disrupted. The results for  $T_g$  were well described by an empirical equation, and we observed that a constant, pressure independent, increase in temperature can roughly account for an increase in molecular weight.

In Paper VIII, a comprehensive investigation of SWCNT and MWCNT filled sPB and LPB was made. The results of  $\kappa$ ,  $T_g$ , interfacial interaction and microstructure before and after HP&HT treatment were reported. The most striking result was that the microstructure of MWCNT/LPB composite changed from randomly dispersed CNTs to a web-like structure of coated and/or wrapped CNTs, with a permanent shift in their Raman D\*-band by as much as  $\sim 16 \text{ cm}^{-1}$ . Moreover,  $\kappa$  of the recovered state of a 2.9 wt% -COOH functionalized MWCNT composite increased by  $\sim 34\%$ , which was attributed to an irreversible densification and a consequentially increased phonon velocity. Due to ebonite like state after HP&HT treatment, the material was too brittle for mechanical tests and therefore no tensile result was reported.

Results prior to treatments showed that the SWCNT fillers promote  $\kappa$  better (17%/wt%CNT) than MWCNT-SH fillers (8%/wt%CNT), which was well accounted for by their higher aspect ratio. The SWCNTs also raised  $T_g$  slightly more than MWCNTs and, in particular, under the most densified conditions and for LPB, which may due to more favorable conditions for coating/wrapping.

In Paper VII, I performed *in-situ* hot-wire measurement for LPB, Raman spectroscopy for sPB and LPB. I also participated in the evaluation and discussions of the manuscript. In Paper VIII, I performed *in-situ* hot-wire measurement for MWCNT/LPB composites, Raman spectroscopy and AFM for MWCNT/LPB composites. Bounphanh Tonpheng performed *in-situ* hot-

wire measurement for SWCNT/LPB, SWCNT/sPB composites. I and Gerhard Gröbner performed NMR analyses of LPB and SWCNT/MWCNT/LPB composites. All authors were involved in evaluation and discussions of the results. I wrote the first version of manuscript together with Ove Andersson.

## **Paper IX**

Paper IX concerned the effects of  $C_{60}$  as a filler in PI.  $C_{60}$  is a football-shaped filler with a diameter of about 1 nm. Because of its shape, it is normally not considered as a filler for reinforcement applications where fillers with high aspect ratio, like that of tubular shaped CNTs, have advantages. However, after HP&HT treatment, the results suggested that  $C_{60}$  was covalently bonded to PI chains, and also covalently bonded to other  $C_{60}$  molecules in  $C_{60}$  clusters. The reinforcement effects by  $C_{60}$  in sPI was large. Moreover, the inter- $C_{60}$ - $C_{60}$  bonds could be broken purely by heating the material at low pressure, and therefore we could partly reverse the mechanical properties of the  $C_{60}$ /sPI composites. This opens possibilities for a new route to recycle cross-linked rubber material using  $C_{60}$  clusters as cross-linkers instead of sulfur, peroxide etc.

The most surprising result in this paper was the mechanical reinforcement provided by  $C_{60}$ . For example, sPI filled with 9.1 wt%  $C_{60}$  showed 5.5 times higher  $\sigma_{UTS}$  and 9 times larger  $E$  than neat sPI after identical HP&HT treatment at 1.5 GPa. NMR results suggested that  $C_{60}$  was covalently bonded to sPI. Moreover, WAXD spectra indicated that there was also  $C_{60}$ - $C_{60}$  bonding. The  $C_{60}$ - $C_{60}$  bonds in the composite could be broken easily by heating at ambient pressure. A sample subjected to this treatment showed decreased tensile performance, decreased cross-link density and reversibility of WAXD spectra, i.e. the original crystalline  $C_{60}$  spectrum recorded before HP&HT treatment was recovered. It followed that the cross-links in the composite were partly reversed. This effect can be optimized with a suitable combination of pressure and temperature for HP&HT treatment and with suitable sizes of  $C_{60}$  clusters as reversible cross-linkers. The best would be to produce maximal reinforcement by  $C_{60}$ - $C_{60}$  bonded clusters and avoid single  $C_{60}$  units as cross-linker between PI chains. Thus,  $C_{60}$  clusters may not only reinforce a composite but also make the reinforcement reversible, indicating that the material can be recycled.

In paper IX, I synthesized the  $C_{60}$ /sPI composites, conducted the HP&HT treatment, tensile tests, WAXD and swelling measurements. I and Gerhard Gröbner performed NMR analyses of the  $C_{60}$ /sPI composite. All authors were involved in the evaluation of the results. I wrote the first version of the manuscript together with Ove Andersson.

## IV. Conclusion and Perspective

### Conclusion

In this thesis work, I have studied the dynamics of two-component systems, or composites, under high pressure conditions and the effect of HP&HT treatment on the thermal and mechanical properties. The systems consisted of small amounts of a nanosized carbon filler (CNTs or C<sub>60</sub>) in a polymer matrix.

The CNTs behaved almost inert in the polymer, i.e. crystallization and cross-link processes induced by HP&HT treatment did not affect the CNTs chemically. But CNTs can: i. act as sites for nucleation and growth (recrystallization) of polymer crystals and thereby enhance the thermal stability; ii. slightly slow down the movements of polymer chains (increase  $T_g$ ) and be wrapped/coated by polymer chains.

The C<sub>60</sub> behaved as an active cross-linker in polyisoprene. At current stage, there is strong evidence that it can be covalently bonded to the polymer chains and to C<sub>60</sub> neighbors as a result of HP&HT treatment.

The following links between the microstructural characteristics of the nanocomposites and the macroscopic properties were found:

i. Adding CNTs into a polymer increases  $\kappa$ , but the increase is limited by a large interfacial thermal resistance between the CNTs and the polymer. The best enhancement of  $\kappa$  observed in this work is 24%/wt% SWCNT in sPI. This is better than for MWCNTs, which is probably because of their higher aspect ratio and not their about 2 times higher  $\kappa$ .

ii. Adding CNTs or C<sub>60</sub> into a polymer provides effective reinforcement if the filler is well dispersed and the polymer is cross-linked at HP&HT conditions, which yields highly densified cross-links. The largest increases of  $\sigma_{UTS}$  achieved in this thesis are 38%/wt% MWCNT and 49%/wt% C<sub>60</sub> in sPI. In the former case, evidence was found for 'bound' polymer in the form of a layer of sPI coated/wrapped on CNTs that can provide an effective load transfer between sPI and the MWCNTs. The reinforcing function of C<sub>60</sub> fillers is different from that of CNTs as C<sub>60</sub> becomes covalently bonded to sPI chains and C<sub>60</sub> clusters in sPI form C<sub>60</sub>-C<sub>60</sub> covalent bonds. The latter are reversible and break by heating at 1 bar, which suggest an improved recyclability of the material.

## Perspective

Considering  $\kappa$  of polymer carbon nanocomposite, the enhancement after adding CNTs is relatively small, which is due to a very large interfacial thermal resistance. However, Haggemueller et al. [70] observed a strong increment of  $\kappa$  at high dosages of CNTs in PE, which they attributed to a well-conducting network of CNTs supported by crystalline bridges of PE. Similar results were reported for randomly dispersed CNTs in different polymer matrices at high CNT loading (ca. 10 vol%). [133] Since we have the advantage of high pressure equipment, it would be an interesting experiment to crystallize a semicrystalline polymer by HP&HT treatment in a high CNT dosage composite. This should increase the possibility for obtaining crystalline bridges in between CNTs. Thus, an *in-situ* study of  $\kappa$  during such experiment may verify the development of a well-conducting network.

As reported in Paper VI, evidence was found for a polymer layer coated/wrapped on CNTs, which can be improved by high pressure treatments. It was also deduced that this layer is important for achieving an effective load transfer between a polymer matrix and CNTs. For example, 3 wt% MWCNT in sPI increased  $\sigma_{\text{UTS}}$  and  $E$  by more than 2 times. In this composite, sPI is a relatively soft and weak matrix. Thus, a study of a polymer with higher initial  $\sigma_{\text{UTS}}$  and  $E$ , which can also be cross-linked by HP&HT treatment, may provide highly interesting results in the attempts to obtain high-strength low-weight composites. Moreover, similar studies as done here but with graphene fillers, which in theory can provide twice as large specific surface area as CNTs, would further illuminate the effect of surface area and geometry on the composites' properties.

In Paper IX,  $\text{C}_{60}$  acts as both strong reinforcer and reversible cross-linker in a rubber material. It would be very interesting to investigate further if the reversible cross-linking process in  $\text{C}_{60}$  clusters can be used to make strong recyclable elastomeric materials.

## **V. Supplementary material**

### **9. Conferences, summer schools and other activities**

#### **9.1 Conference**

5<sup>th</sup> International conference on Times of Polymers (TOP) & Composites, 20-23 June 2010, Ischia, Italy

- ❖ Oral presentation: Thermal conductivity and heat capacity of a nylon-6/multiwall carbon nanotube composite under pressure

#### **9.2 Summer school**

1. Insight into the Soft Matter through bio/non-bio interactions

June 29-July 3, 2008, Hönö, Sweden

Course Responsible: Alexandre Dmitriev (Chalmers)

2. NMR - basic physics and applications

August, 25-28, 2008, Fiskebäckskil, Sweden

Course responsible: Magnus Nydén (Chalmers)

#### **9.3 Student networking activities**

1. Kick-off meeting for Chalmers Soft Matter Graduate School

April, 17-18, 2008, Hjortviken, Sweden

Organizers: Krister Holmberg and Aleksandar Matic (Chalmers)

2. Graduate students workshop

September 10-12, 2008, Onsala herrgård, Onsala, Sweden

Organizers: Jonas Nordström and Philip Karlsson (Chalmers)

## Acknowledgements

This doctoral thesis was performed at the Dept. of Physics, Umeå University in Umeå, Sweden from Jul, 2007 to Dec, 2011. I have enjoyed my time here in both study and life. I have received much supports and encouragements I will treasure for years.

First of all, I would like to express my deepest gratitude to my supervisor Assoc. Prof. Ove Andersson. There are so many words I want to say but can only briefly write a few down. I feel so lucky to be admitted and work with you as a PhD student. Your rigorous attitude towards science and research influences me a lot. Your inspirational and thoughtful ideas always inspire me. Besides the knowledge and sophisticated experimental skills, your pedagogical skill, patience and kindness make a perfect mentor for me. Without your delicate work, continuous support, friendliness and invaluable suggestions, this journey would probably not have been so productive and so fast.

I would like to thank my Co-supervisor Prof. Bertil Sundqvist. I benefit a lot from your expertise in fullerenes material, lab experience, countless help with high-pressure equipment, Raman, WAXD, glove box and other stuffs I cannot list them all here. Thanks for always creating a positive and relaxing atmosphere in the experimental hall.

I would like to show my gratitude to Prof. Gerhard Gröbner from Dept. of Chemistry, who introduced me to the NMR techniques and later became an active co-author in many of my publications. Your expertise in NMR provided important pieces of information to finish my puzzle. Special thanks for correcting the NMR section of my thesis.

Senior researchers in the department gave me a lot of useful advices and help during my stay. I wish to specially thank Thomas Wågberg, Alexandr Talyzin, Tatiana Makarova and Ludvig Edman here. Hans Forsman is acknowledged for giving me the opportunity for teaching.

My special thanks to workshop staffs, Lena Åström and Tomas Gustafsson. My experiments could not run smoothly without your help. Thanks for many smart tools/designs/techniques making life much easier and ideal in the lab. Leif Hassmyr is acknowledged for lending me many useful equipments for different projects. Lars-Erik Svensson, Nils Blix and Lars Karlsson are acknowledged for keeping computer/electronic devices healthy.

I met many (former) PhD students and Post-docs here and fortunately also many Chinese friends. I would like to thank Bounphanh, Agnieszka, Patrik, Mats, Serhiy, Florian, Hamid, Valeria, Daniel, Mingguang, Junfeng,

Weiguang, Jie, Zhi-xi, Jia, Shi, Junyang, Guangzhi and Shujie for interesting discussion/advice about project, equipment, holidays etc.

I believe my daily life in Physics is easy because of 2 main reasons: (a) thanks for highly efficient administrators: Katarina Hassler, Lena Burström, Ann-Charlott Dalberg and Lilian Andersson; (b) thanks Jörgen Eriksson for taking good care of other non-standard, I don't know who to ask types of questions. Dept. of Physics always gives me a feeling of warmth, openness and friendliness; I would like to express my gratitude to all of you here for creating a wonderful atmosphere at work.

Nanotechnology is an inter-discipline subject, which I can also prove here. I thank for Åke Fransson for coaching me DSC and Britt Andersson for teaching me SEM, both at the Dept. of Applied Physics and Electronics; I thank Lenore Johansson for instruction of using TEM & ultramicrotome and Tobias Sparrman for help with the NMR spectrometer, both at the Dept. of Chemistry. The workshops held at KBC and UCMR were very helpful for learning various microscope techniques and English writing.

Outside of science life, I formed a healthy habit to do sports frequently in Umeå (IKSU!). I met a lot of fanatical football fans here with endless energy to run and score. I enjoyed having this crazy hour(s) every week playing football together. Besides, I have some friends from Dept. of Economics to play badminton occasionally. Recently, I had a nice time to join my friends from UPSC to play innebandy. Here I would like to thank all of you for being good companions.

It is very important to have the support from my family. Thanks to my wife Yuna, my life can not have color without you. You are acknowledged not only for being an excellent life partner but also for proof reading of my thesis;) My parents are acknowledged for always understanding, supporting and encouraging my studies. I met Gunilla and Elie Najjar when I first arrived in Sweden, thanks for your caring and kindness, and for being positive all the time.☺

Junchun Yu  
2011-10-30 Umeå  
Sweden

## References

- [1] <http://en.wikipedia.org/wiki/Carbon>.
- [2] Ajayan PM. Nanotubes from Carbon. *Chem Rev* 1999; 99(7):1787-800.
- [3] Echegoyen L, Echegoyen LE. Electrochemistry of Fullerenes and Their Derivatives. *Acc Chem Res* 1998; 31(9):593-601.
- [4] Novoselov KS, Geim AK, Morozov SV, Jiang D, Zhang Y, Dubonos SV, et al. Electric Field Effect in Atomically Thin Carbon Films. *Science* 2004; 306(5696):666-9.
- [5] Shaffer MSP, Sandler JKW. Carbon Nanotube/Nanofibre Polymer Composites: World Scientific Publishing Co.: 1-59.
- [6] Kroto HW, Heath JR, O'Brien SC, Curl RF, Smalley RE. C60: Buckminsterfullerene. *Nature* 1985; 318(6042):162-3.
- [7] Iijima S. Helical microtubules of graphitic carbon. *Nature* 1991; 354(6348):56-8.
- [8] Iijima S, Ichihashi T. Single-shell carbon nanotubes of 1-nm diameter. *Nature* 1993; 363(6430):603-5.
- [9] Andrews R, Jacques D, Qian D, Rantell T. Multiwall Carbon Nanotubes: Synthesis and Application. *Acc Chem Res* 2002; 35(12):1008-17.
- [10] Karousis N, Tagmatarchis N, Tasis D. Current Progress on the Chemical Modification of Carbon Nanotubes. *Chem Rev* 2010; 110(9):5366-97.
- [11] Sun Y-P, Fu K, Lin Y, Huang W. Functionalized Carbon Nanotubes: Properties and Applications. *Acc Chem Res* 2002; 35(12):1096-104.
- [12] Zhao Y-L, Stoddart JF. Noncovalent Functionalization of Single-Walled Carbon Nanotubes. *Acc Chem Res* 2009; 42(8):1161-71.
- [13] Moniruzzaman M, Winey KI. Polymer Nanocomposites Containing Carbon Nanotubes. *Macromolecules* 2006; 39(16):5194-205.
- [14] Baughman RH, Zakhidov AA, de Heer WA. Carbon Nanotubes--the Route Toward Applications. *Science* 2002; 297(5582):787-92.
- [15] Ajayan PM, Tour JM. Materials Science: Nanotube composites. *Nature* 2007; 447(7148):1066-8.
- [16] Ajayan P, Zhou O, Dresselhaus M, Dresselhaus G, Avouris P. Applications of Carbon Nanotubes in Carbon nanotubes. Springer Berlin / Heidelberg 2001, p. 391-425.
- [17] Endo M, Strano M, Ajayan P. Potential Applications of Carbon Nanotubes in Carbon Nanotubes. Springer Berlin / Heidelberg 2008, p. 13-61.
- [18] Schnorr JM, Swager TM. Emerging Applications of Carbon Nanotubes. *Chem Mater* 2011; 23(3):646-57.
- [19] Berber S, Kwon Y-K, Tománek D. Unusually High Thermal Conductivity of Carbon Nanotubes. *Phys Rev Lett* 2000; 84(20):4613.
- [20] Donadio D, Galli G. Thermal Conductivity of Isolated and Interacting Carbon Nanotubes: Comparing Results from Molecular Dynamics and the Boltzmann Transport Equation. *Phys Rev Lett* 2007; 99(25):255502.
- [21] Fujii M, Zhang X, Xie H, Ago H, Takahashi K, Ikuta T, et al. Measuring the Thermal Conductivity of a Single Carbon Nanotube. *Phys Rev Lett* 2005; 95(6):065502.
- [22] Kim P, Shi L, Majumdar A, McEuen PL. Thermal Transport Measurements of Individual Multiwalled Nanotubes. *Phys Rev Lett* 2001; 87(21):215502.

- [23] Xia Y, Zhao M, Ma Y, Ying M, Liu X, Liu P, et al. Tensile strength of single-walled carbon nanotubes with defects under hydrostatic pressure. *Phys Rev B* 2002; 65(15):155415.
- [24] Liew KM, He XQ, Wong CH. On the study of elastic and plastic properties of multi-walled carbon nanotubes under axial tension using molecular dynamics simulation. *Acta Mater* 2004; 52(9):2521-7.
- [25] Yu M-F, Files BS, Arepalli S, Ruoff RS. Tensile Loading of Ropes of Single Wall Carbon Nanotubes and their Mechanical Properties. *Phys Rev Lett* 2000; 84(24):5552.
- [26] Yu M-F, Lourie O, Dyer MJ, Moloni K, Kelly TF, Ruoff RS. Strength and Breaking Mechanism of Multiwalled Carbon Nanotubes Under Tensile Load. *Science* 2000; 287(5453):637-40.
- [27] Lu JP. Elastic Properties of Carbon Nanotubes and Nanoropes. *Phys Rev Lett* 1997; 79(7):1297.
- [28] Sinnott SB, Shenderova OA, White CT, Brenner DW. Mechanical properties of nanotubule fibers and composites determined from theoretical calculations and simulations. *Carbon* 1998; 36(1-2):1-9.
- [29] Treacy MMJ, Ebbesen TW, Gibson JM. Exceptionally high Young's modulus observed for individual carbon nanotubes. *Nature* 1996; 381(6584):678-80.
- [30] Peigney A, Laurent C, Flahaut E, Bacsa RR, Rousset A. Specific surface area of carbon nanotubes and bundles of carbon nanotubes. *Carbon* 2001; 39(4):507-14.
- [31] Ye Y, Ahn CC, Witham C, Fultz B, Liu J, Rinzler AG, et al. Hydrogen adsorption and cohesive energy of single-walled carbon nanotubes. *Appl Phys Lett* 1999; 74(16):2307-9.
- [32] Inoue S, Ichikuni N, Suzuki T, Uematsu T, Kaneko K. Capillary Condensation of N<sub>2</sub> on Multiwall Carbon Nanotubes. *J Phys Chem B* 1998; 102(24):4689-92.
- [33] Lee RS, Kim HJ, Fischer JE, Thess A, Smalley RE. Conductivity enhancement in single-walled carbon nanotube bundles doped with K and Br. *Nature* 1997; 388(6639):255-7.
- [34] Ebbesen TW, Lezec HJ, Hiura H, Bennett JW, Ghaemi HF, Thio T. Electrical conductivity of individual carbon nanotubes. *Nature* 1996; 382(6586):54-6.
- [35] Chae HG, Liu J, Kumar S. *Carbon Nanotubes, Properties and Applications*. Boca Raton: CRC Press; 2006: 214-52.
- [36] Dresselhaus MS, Dresselhaus G, Avouris P. *Carbon Nanotubes: Synthesis, Structure, Properties, and Applications*. Berlin Heidelberg: Springer-Verlag; 2001: 448.
- [37] Hone J, Llaguno MC, Biercuk MJ, Johnson AT, Batlogg B, Benes Z, et al. Thermal properties of carbon nanotubes and nanotube-based materials. *Appl Phys A: Mater Sci Process* 2002; 74(3):339-43.
- [38] Yang DJ, Zhang Q, Chen G, Yoon SF, Ahn J, Wang SG, et al. Thermal conductivity of multiwalled carbon nanotubes. *Phys Rev B* 2002; 66(16):165440.
- [39] Yi W, Lu L, Dian-lin Z, Pan ZW, Xie SS. Linear specific heat of carbon nanotubes. *Phys Rev B* 1999; 59(14):R9015.
- [40] Coleman JN, Khan U, Blau WJ, Gun'ko YK. Small but strong: A review of the mechanical properties of carbon nanotube-polymer composites. *Carbon* 2006; 44(9):1624-52.

- [41] Dai H. Carbon Nanotubes: Synthesis, Integration, and Properties. *Acc Chem Res* 2002; 35(12):1035-44.
- [42] Ebbesen TW, Ajayan PM. Large-scale synthesis of carbon nanotubes. *Nature* 1992; 358(6383):220-2.
- [43] Hata K, Futaba DN, Mizuno K, Namai T, Yumura M, Iijima S. Water-Assisted Highly Efficient Synthesis of Impurity-Free Single-Walled Carbon Nanotubes. *Science* 2004; 306(5700):1362-4.
- [44] Moon J-M, An KH, Lee YH, Park YS, Bae DJ, Park G-S. High-Yield Purification Process of Singlewalled Carbon Nanotubes. *J Phys Chem B* 2001; 105(24):5677-81.
- [45] Giacalone F, Martan N. Fullerene Polymers: Synthesis and Properties. *Chem Rev* 2006; 106(12):5136-90.
- [46] Iwasiewicz-Wabnig A. Studies of carbon nanomaterials based on fullerenes and carbon nanotubes. Umea University, Doctoral, 2007.
- [47] Sundqvist B. Polymeric Fullerene Phases Formed Under Pressure. *Fullerene-Based Materials: Springer Berlin / Heidelberg* 2004, p. 85-126.
- [48] Blank VD, Buga SG, Dubitsky GA, R. Serebryanaya N, Popov MY, Sundqvist B. High-pressure polymerized phases of C<sub>60</sub>. *Carbon* 1998; 36(4):319-43.
- [49] Gedde UW. *Polymer Physics* Dordrecht: Kluwer Academic Publishers; 2001:
- [50] <http://en.wikipedia.org/wiki/Polymer>.
- [51] Kohan MI. *Nylon Plastics Handbook*. Cincinnati: Hanser/Gardner Publications, Inc. ; 1995:
- [52] Yu J, Tonpheng B, Andersson O. High-Pressure-Induced Microstructural Evolution and Enhancement of Thermal Properties of Nylon-6. *Macromolecules* 2010; 43(24):10512-20.
- [53] <http://en.wikipedia.org/wiki/Polyisoprene>.
- [54] Miles DC, Briston JH. *Polymer technology*. London: Temple press; 1965: 285.
- [55] Merwe MJVD, Gradwell MHS, McGill WJ. Influence of pendent groups on the tensile properties of polyisoprene vulcanizates. *J Appl Polym Sci* 2001; 81(11):2587-96.
- [56] Tonpheng B, Andersson O. Crosslinking, thermal properties and relaxation behaviour of polyisoprene under high-pressure. *Eur Polym J* 2008; 44(9):2865-73.
- [57] <http://en.wikipedia.org/wiki/Polybutadiene>.
- [58] Tonpheng B, Yu J, Andersson O. Effects of cross-links, pressure and temperature on the thermal properties and glass transition behaviour of polybutadiene. *Phys Chem Chem Phys* 2011; 13(33):15047-54.
- [59] Bellander M, Stenberg B, Persson S. Crosslinking of polybutadiene rubber without any vulcanization agent. *Polym Eng Sci* 1998; 38(8):1254-60.
- [60] [http://en.wikipedia.org/wiki/Composite material](http://en.wikipedia.org/wiki/Composite_material).
- [61] Hull D, Clyne TW. *An introduction to composite materials*. 2nd ed. Cambridge: Cambridge University Press; 1996:
- [62] Frisch HL, Mark JE. Nanocomposites Prepared by Threading Polymer Chains through Zeolites, Mesoporous Silica, or Silica Nanotubes. *Chem Mater* 1996; 8(8):1735-8.
- [63] Bose S, Khare RA, Moldenaers P. Assessing the strengths and weaknesses of various types of pre-treatments of carbon nanotubes on the properties of polymer/carbon nanotubes composites: A critical review. *Polymer* 2010; 51(5):975-93.

- [64] Bhattacharyya S, Sinturel C, Bahloul O, Saboungi M-L, Thomas S, Salvétat J-P. Improving reinforcement of natural rubber by networking of activated carbon nanotubes. *Carbon* 2008; 46(7):1037-45.
- [65] Sui X, Wagner HD. Tough Nanocomposites: The Role of Carbon Nanotube Type. *Nano Lett* 2009; 9(4):1423-6.
- [66] Moniruzzaman M, Chattopadhyay J, Billups WE, Winey KI. Tuning the Mechanical Properties of SWNT/Nylon 6,10 Composites with Flexible Spacers at the Interface. *Nano Lett* 2007; 7(5):1178-85.
- [67] Ma W, Liu L, Zhang Z, Yang R, Liu G, Zhang T, et al. High-Strength Composite Fibers: Realizing True Potential of Carbon Nanotubes in Polymer Matrix through Continuous Reticulate Architecture and Molecular Level Couplings. *Nano Lett* 2009; 9(8):2855-61.
- [68] Deng F, Lu W, Zhao H, Zhu Y, Kim B-S, Chou T-W. The properties of dry-spun carbon nanotube fibers and their interfacial shear strength in an epoxy composite. *Carbon* 2011; 49(5):1752-7.
- [69] Yang Y. *Physical properties of polymer handbook*. 2nd ed. New York: Springer-Verlag; 2007: 155-64.
- [70] Haggemueller R, Guthy C, Lukes JR, Fischer JE, Winey KI. Single Wall Carbon Nanotube/Polyethylene Nanocomposites: Thermal and Electrical Conductivity. *Macromolecules* 2007; 40(7):2417-21.
- [71] Nan C-W, Liu G, Lin Y, Li M. Interface effect on thermal conductivity of carbon nanotube composites. *Appl Phys Lett* 2004; 85(16):3549-51.
- [72] Nan C-W, Birringer R, Clarke DR, Gleiter H. Effective thermal conductivity of particulate composites with interfacial thermal resistance. *J Appl Phys* 1997; 81(10):6692-9.
- [73] Nan CW, Shi Z, Lin Y. A simple model for thermal conductivity of carbon nanotube-based composites. *Chem Phys Lett* 2003; 375(5-6):666-9.
- [74] Huxtable ST, Cahill DG, Shenogin S, Xue L, Ozisik R, Barone P, et al. Interfacial heat flow in carbon nanotube suspensions. *Nat Mater* 2003; 2(11):731-4.
- [75] Xu Z, Buehler MJ. Nanoengineering Heat Transfer Performance at Carbon Nanotube Interfaces. *ACS Nano* 2009; 3(9):2767-75.
- [76] Kropka JM, Garcia Sakai V, Green PF. Local Polymer Dynamics in Polymer-C<sub>60</sub> Mixtures. *Nano Lett* 2008; 8(4):1061-5.
- [77] Kropka JM, Putz KW, Pryamitsyn V, Ganesan V, Green PF. Origin of Dynamical Properties in PMMA-C<sub>60</sub> Nanocomposites. *Macromolecules* 2007; 40(15):5424-32.
- [78] Yang C, Hu JG, Heeger AJ. Molecular Structure and Dynamics at the Interfaces within Bulk Heterojunction Materials for Solar Cells. *J Am Chem Soc* 2006; 128(36):12007-13.
- [79] Wu C-S. Preparation and characterization of a polycaprolactone/C<sub>60</sub> composite and its improved counterpart (PCL-NH<sub>2</sub>/C<sub>60</sub>-OH). *J Appl Polym Sci* 2010; 115(6):3489-99.
- [80] Gao J, Itkis ME, Yu A, Bekyarova E, Zhao B, Haddon RC. Continuous Spinning of a Single-Walled Carbon Nanotube-Nylon Composite Fiber. *J Am Chem Soc* 2005; 127(11):3847-54.
- [81] Gao J, Zhao B, Itkis ME, Bekyarova E, Hu H, Kranak V, et al. Chemical Engineering of the Single-Walled Carbon Nanotube-Nylon 6 Interface. *J Am Chem Soc* 2006; 128(23):7492-6.

- [82] Hu L, Hecht DS, Gruner G. Carbon Nanotube Thin Films: Fabrication, Properties, and Applications. *Chem Rev* 2010; 110(10):5790-844.
- [83] Andersson P. Specific heat, thermal conductivity and thermal diffusivity of solids at high pressures. Umeå University, Doctoral, 1973.
- [84] Alm O. Thermal conductivity of insulating solids under pressure. Umeå University, Doctoral, 1976.
- [85] Håkansson B. Thermal conductivity of alkali halides under pressure. Umeå University, Doctoral, 1989.
- [86] Kittel C. Introduction to solid state physics. 8th ed: John Wiley & Sons, Inc.; 2005: 121-8.
- [87] Håkansson B, Andersson P, Backstrom G. Improved hot-wire procedure for thermophysical measurements under pressure. *Rev Sci Instrum* 1988; 59(10):2269-75.
- [88] Carslaw HS, Jaeger JS. Conduction of heat in solids. 2nd ed. Clarendon: Oxford University Press 1959, p. 341.
- [89] Sandberg O. Thermal properties of organic glass formers under pressure. Umeå University, Doctoral, 1980.
- [90] Andersson O. Thermal conductivity and phase diagram of organic substances under pressure. Umeå University, Doctoral, 1991.
- [91] Tonpheng B. Thermal and mechanical studies of carbon nanotube-polymer composites synthesized at high pressure and high temperature. Umeå University, Doctoral, 2011.
- [92] Nielsen LE, Landel RF. Mechanical properties of polymers and composites. 2nd ed. New York: Marcel Dekker; 1994:
- [93] Yu J, Tonpheng B, Gröbner G, Andersson O. A MWCNT/polyisoprene composite reinforced by an effective load transfer reflected in the extent of polymer coating. Submitted.
- [94] Tonpheng B, Yu J, Andersson BM, Andersson O. Tensile Strength and Young's Modulus of Polyisoprene/Single-Wall Carbon Nanotube Composites Increased by High Pressure Cross-linking. *Macromolecules* 2010; 43(18):7680-8.
- [95] [http://en.wikipedia.org/wiki/High-resolution\\_transmission\\_electron\\_microscopy](http://en.wikipedia.org/wiki/High-resolution_transmission_electron_microscopy).
- [96] [http://en.wikipedia.org/wiki/Scanning\\_electron\\_microscope](http://en.wikipedia.org/wiki/Scanning_electron_microscope).
- [97] [http://en.wikipedia.org/wiki/Transmission\\_electron\\_microscope](http://en.wikipedia.org/wiki/Transmission_electron_microscope).
- [98] Meyer E, Hug HJ, Bennewitz R. Scanning Probe Microscopy: The lab on a tip. Berlin: Springer; 2004:
- [99] Magonov SN, Whangbo M-H. Surface Analysis with STM and AFM: Experimental and Theoretical Aspects of Image Analysis. Weinheim: John Wiley & Sons, Inc.; 2008:
- [100] Dong R, Yu LE. Investigation of Surface Changes of Nanoparticles Using TM-AFM Phase Imaging. *Environ Sci Technol* 2003; 37(12):2813-9.
- [101] García R, Pérez R. Dynamic atomic force microscopy methods. *Surf Sci Rep* 2002; 47(6-8):197-301.
- [102] Tamayo J, García R. Deformation, Contact Time, and Phase Contrast in Tapping Mode Scanning Force Microscopy. *Langmuir* 1996; 12(18):4430-5.
- [103] Tamayo J, García R. Effects of elastic and inelastic interactions on phase contrast images in tapping-mode scanning force microscopy. *Appl Phys Lett* 1997; 71:2394-6.

- [104] Reid N, Beesly JE. Sectioning and cryosectioning for electron microscopy. Amsterdam: Elsevier; 1991:
- [105] Goodhew PJ. Thin foil preparation for electron microscopy. Amsterdam: Elsevier; 1985:
- [106] Ando I, Asakura T. Solid state NMR of polymers. Amsterdam: Elsevier; 1998:
- [107] Stenman K. Prostate cancer diagnosis: experimental and clinical studies with HRMAS NMR spectroscopy. Umeå University, Doctoral, 2011.
- [108] Jacobsen NE. NMR Spectroscopy Explained: Simplified Theory, Applications and Examples for Organic Chemistry and Structural Biology. New Jersey: John Wiley&Sons, Inc.; 2007:
- [109] Spiess HW. Structure and dynamics of solid polymers from 2D- and 3D-NMR. Chem Rev 1991; 91(7):1321-38.
- [110] Yu J, Gröbner G, Tonpheng B, Andersson O. Buckminsterfullerene: A strong, covalently bonded, reinforcing filler and reversible cross-linker in the form of clusters in a polymer. In manuscript.
- [111] Lindström F. Biological membrane interfaces involved in diseases: a biophysical study. Umeå University, Doctoral, 2006.
- [112] Yu J, Tonpheng B, Gröbner G, Andersson O. Thermal properties and transition studies of multi-wall carbon nanotube/nylon-6 composites. Carbon 2011; 49(14):4858-66.
- [113] Yu J, Gröbner G, Tonpheng B, Andersson O. Microstructure, nucleation and thermal properties of high-pressure crystallized MWCNT/nylon-6 composites. Polymer 2011; 52(24):5521-7.
- [114] Wågberg T. Studies of polymeric and intercalated phases of C<sub>60</sub>. Umeå University, Doctoral, 2001.
- [115] Dresselhaus MS, Dresselhaus G, Jorio A. Raman Spectroscopy of Carbon Nanotubes in 1997 and 2007. J Phys Chem C 2007; 111(48):17887-93.
- [116] Dresselhaus MS, Jorio A, Hofmann M, Dresselhaus G, Saito R. Perspectives on Carbon Nanotubes and Graphene Raman Spectroscopy. Nano Lett 2010; 10(3):751-8.
- [117] Zhao Q, Daniel Wagner H. Two-dimensional strain mapping in model fiber-polymer composites using nanotube Raman sensing. Composites Part A 2003; 34(12):1219-25.
- [118] Lourie O, Wagner HD. Evaluation of Young's Modulus of Carbon Nanotubes by Micro-Raman Spectroscopy. J Mater Res 1998; 13(09):2418-22
- [119] Yu J, Tonpheng B, Gröbner G, Andersson O. Microstructural and property changes in high pressure treated carbon nanotube/polybutadiene composites. J Mater Chem 2011; 21(35):13672-82.
- [120] Valentin JL, Carretero-Gonzalez J, Mora-Barrantes I, Chasse W, Saalwächter K. Uncertainties in the Determination of Cross-Link Density by Equilibrium Swelling Experiments in Natural Rubber. Macromolecules 2008; 41(13):4717-29.
- [121] Tonpheng B, Yu J, Andersson O. Thermal Conductivity, Heat Capacity, and Cross-Linking of Polyisoprene/Single-Wall Carbon Nanotube Composites under High Pressure. Macromolecules 2009; 42(23):9295-301.
- [122] Flory PJ. Statistical Mechanics of Swelling of Network Structures. J Chem Phys 1950; 18(1):108-11.
- [123] Flory PJ, John Rehner J. Statistical Mechanics of Cross-Linked Polymer Networks I. Rubberlike Elasticity. J Chem Phys 1943; 11(11):512-20.

- [124] Horkay F, McKenna GB, Deschamps P, Geissler E. Neutron Scattering Properties of Randomly Cross-Linked Polyisoprene Gels. *Macromolecules* 2000; 33(14):5215-20.
- [125] Orwoll RA. The polymer-solvent interaction parameter  $\chi$ . *Rubber Chem Technol* 1977; 50(3):451-79.
- [126] Gent AN, Kaang SY. Diffusion of linear polyisoprene molecules into polyisoprene networks. *J Polym Sci Part B: Polym Phys* 1989; 27(4):893-911.
- [127] Sengupta R, Sabharwal S, Tikku VK, Somani AK, Chaki TK, Bhowmick AK. Effect of ambient-temperature and high-temperature electron-beam radiation on the structural, thermal, mechanical, and dynamic mechanical properties of injection-molded polyamide-6,6. *J Appl Polym Sci* 2006; 99(4):1633-44.
- [128] Schaeffgen JR, Flory PJ. Synthesis of Multichain Polymers and Investigation of their Viscosities. *J Am Chem Soc* 1948; 70(8):2709-18.
- [129] Mattiussi A, Gechele GB, Francesconi R. Polyamides in solution. III. Viscometry of linear polycaprolactam. *J Polym Sci, Part A-2: Polym Phys* 1969; 7(2):411-22.
- [130] HAAKE Falling Ball Viscometer type B manual:
- [131] Isasi JR, Mandelkern L, Galante MJ, Alamo RG. The degree of crystallinity of monoclinic isotactic poly(propylene). *J Polym Sci Part B: Polym Phys* 1999; 37(4):323-34.
- [132] Bellander M. Crosslinking of Diene Rubbers Without Vulcanization Agents. Royal Institute of Technology, Doctoral, 1998.
- [133] Marconnet AM, Yamamoto N, Panzer MA, Wardle BL, Goodson KE. Thermal Conduction in Aligned Carbon Nanotube-Polymer Nanocomposites with High Packing Density. *ACS Nano* 2011; 5(6):4818-25.